Journal of Structural Geology 187 (2024) 105239

Contents lists available at ScienceDirect

Journal of Structural Geology

journal homepage: www.elsevier.com/locate/jsg

Active strike-slip faulting, diapirism and seismic hazards. The case of the Kareh Bas fault and the associated Dandenjan salt extrusion in the zagros Mountains, SW Iran

Francisco Gutiérrez [a,*], Issa Ilyati [b], Mohsen Rezaei [b], Mehdi Zarei [b], Michael Hudec [c]

[a] Department of Earth Sciencies, University of Zaragoza, Pedro Cerbuna 12, 50009, Zaragoza, Spain
[b] Department of Earth Sciences, School of Science, Shiraz University, Shiraz, Iran
[c] Bureau of Economic Geology, Jackson School of Sciences, The University of Texas at Austin, Box X, Austin, TX, 78713-8924, USA

ARTICLE INFO

Keywords:
Precursor diapir
Fault segmentation
Pull-apart basin
Diapiric geomorphology
Earthquake-induced landslides

ABSTRACT

Strike-slip salt diapir systems have been scarcely investigated and have probably been underrecognized. The western Fars Arc of the Zagros Mountains hosts the most remarkable example of salt extrusions associated with seismogenic strike-slip faults within an oblique collisional setting. This study, mainly based on field mapping and observations carried out in the Kareh Bas fault system and the Dandenjan Diapir, explores several issues with practical implications related to these active fault-salt systems: (1) role of precursor diapirs on the initiation of shortening structures; (2) fault segmentation controlled by precursor diapirs, emergence of diapirs, and the development of pull-apart basins; (3) the relative timing of emergence of salt extrusions associated with a propagating strike-slip fault; (4) Quaternary deformation and paleoseismic evidence associated with the Kareh Bas fault; (5) the impact of the salt detachment depth on the seismogenic potential of the segmented Kareh Bas fault system; and (6) clustering of large potentially coseismic landslides in the vicinity of the Kareh Bas fault system.

1. Introduction

The Zagros Fold and Thrust Belt, related to the collision between the Arabian and Eurasian plates, is a paradigmatic example of an orogen with magnificently exposed active deformation structures. The SW-propagating shortening structures in the Zagros foreland display significant along-strike structural variability (e.g., position of the deformation front, taper angle, fold geometry; Molinaro et al., 2005; Macedo and Marshak, 1999; Jahani et al., 2009). This variability is determined by variations in the distribution and thickness of two evaporitic detachments (Sepehr and Cosgrove, 2004): (1) the deep and ca. 1–1.5 km thick Hormuz salt of late Neoproterozoic-early Cambrian age (Kent, 1979; Talbot and Alavi, 1996; Jahani et al., 2017); and (2) the shallow Miocene age Gachsaran Formation. In the southeastern sector of the Zagros foreland, deformation driven by oblique convergence is accommodated through strain partitioning, including orogen-parallel shortening structures (Hormuz-detached folds and basement reverse faults), and oblique N- to NNW-oriented dextral strike-slip faults (Fig. 1) (Authemayou et al., 2006). The most important strike-slip faults are the Kazerun-Borazjan fault system at the western edge of the Fars Arc, and the Kareh-Bas (or Mengarak) fault system (Bachmanov et al., 2004; Authemayou et al., 2009), both more than 200 km long and with horizontal slip rates of around 3.5 mm/yr according to GPS measurements (Tavakoli et al., 2008). There are some relationships between these faults and the evaporitic detachments with important structural and practical implications. The Kazerun-Borazjan fault system is considered to be surface reflection of a major basement fault with long-sustained paleogeographic impact. It controlled the western edge of the extensional Hormuz salt basin (Talbot and Alavi, 1996; Sepehr and Cosgrove, 2004, 2005; Jahani et al., 2017), bounding domains with contrasting basal friction (Cotton and Koyi, 2000). It also defines a significant change in the Gachsaran Formation, with greater thickness and high proportion of halite to the west (i.e., Dezful Embayment), where it plays the role of a shallow detachment (Bahroudi and Koyi, 2004; Sherkati et al., 2005; Ghanadian et al., 2017a, 2017b), and locally produces emergent salt structures (Edgell, 1996; Gutiérrez and Lizaga, 2016). Here, the Gachsaran evaporites act as the seal for reservoirs in the Asmari limestone, which hosts a great part of the oil reserves in the

* Corresponding author.
E-mail address: fgutier@unizar.es (F. Gutiérrez).

https://doi.org/10.1016/j.jsg.2024.105239
Received 7 June 2024; Received in revised form 18 August 2024; Accepted 20 August 2024
Available online 22 August 2024

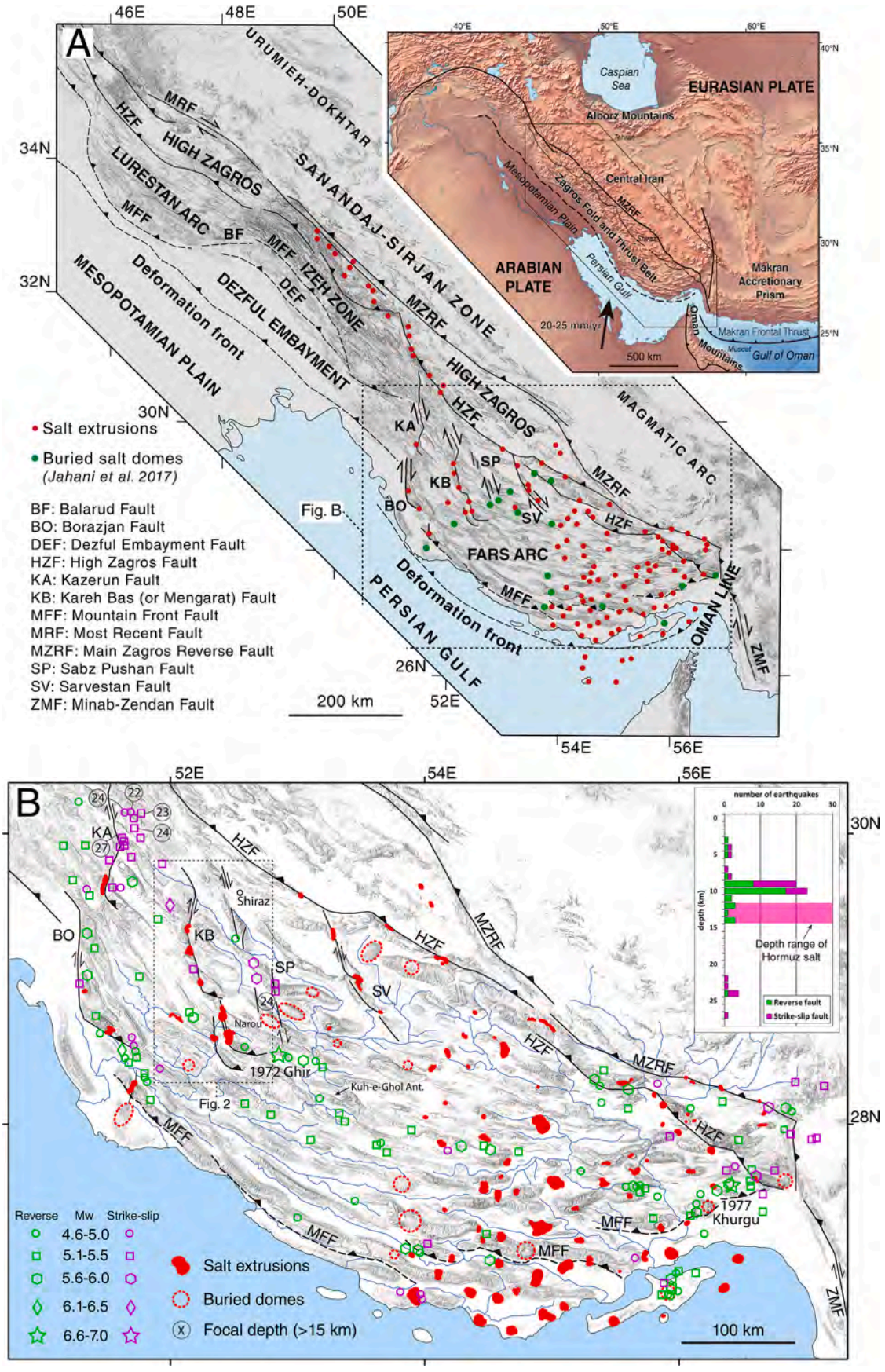

(caption on next page)

Fig. 1. A: Geotectonic setting of the Zagros Fold and Thrust Belt related to the ongoing oblique convergence between the Arabian and Eurasian plates (upper right) and sketch of the Zagros orogen (lower left) showing the distribution of the main structural zones, faults, and salt diapirs, both emerged and buried. Vector displacement of the Arabian Plate from GPS data published by Vernant et al. (2004). B: Map of the Fars Arc of the Simply Folded Belt showing the diapirs of Hormuz salt (emergent and buried), the main faults (names indicated in figure A), and the epicentres from the relocated earthquake catalog (1962–2018; error <5 km) of Karasözen et al. (2019), differentiated by the dominant focal mechanism and M_w (moment magnitude) intervals. Inset shows the distribution of focal depths in the western Fars Arc, between 51°E and 53.5°E, and the depth range of Hormuz salt (ca. 12–15 km) inferred by Jahani et al. (2009, 2017) on the basis of seismic profiles. The focal depths greater to 15 km are indicated in the map by encircled numbers.

region (Bordenave and Hegre, 2010).

The majority of the Hormuz salt extrusions in the western sector of the Fars Arc, which display variable morphological evolutionary stages, are associated with these strike-slip fault systems, representing the most remarkable example of emergent diapirs linked to strike-slip faults worldwide (Jackson and Hudec, 2017). These are widely considered as precursor diapirs rejuvenated during the Zagros orogeny (e.g., Jahani et al., 2009, 2017; Adineh et al., 2023; Ezzati Asl et al., 2019; Faghih et al., 2019). The mechanically weak pre-shortening diapirs have played a major role in the development of deformation structures during the Zagros collision, advancing the onset of deformation, enhancing strain, and guiding the nucleation and propagation path of folds and strike-slip faults (e.g., Callot et al., 2007; Jahani et al., 2009, 2017). However, the mechanical relationships between the south-propagating strike-slip faults and the diapirs have received a variety of interpretations (e.g., Koyi et al., 2008; Talbot and Alavi, 1996; Jahani et al., 2017; Hassanpour et al., 2018), and most studies suffer from the lack of specific field mapping. Strike-slip salt systems are poorly understood, and the available conceptual models are largely based on physical experiments that mostly reproduce the transfer of deformation above pre-existing basement faults (Dooley and Schreurs, 2012; Jackson and Hudec, 2017).

The Zagros orogen is one of the most seismically active mountain belts in the world. However, neotectonic and paleoseismological studies are rather limited, largely because the evaporitic detachments function as barriers preventing the development of coseismic surface ruptures (Berberian 1995; Molinaro et al., 2005). The surface strike-slip faults decorated with salt extrusions in the western Fars Arc constitute an exception. These are potential sources for large earthquakes that may have significant impact on large cities such as Shiraz (1.6 million inhabitants), largely destroyed in 1853 (9000–11,000 fatalities). An additional earthquake-related hazard is the development of coseismic landslides that may reach exceptionally high volumes, velocities and runout in the Zagros Mountains (e.g., rock avalanches; Roberts and Evans, 2013; Gutiérrez et al., 2023a). Despite the great importance of the strike-slip faults from the seismic hazard perspective, the available data for the assessment of their seismogenic potential is poor. Valuable contributions on the Kazerun-Borazjan fault system have been published (Bachmanov et al., 2004; Authemayou et al., 2009), but information on the Kareh Bas fault system is lacking, to the point that no evidence of Quaternary deformation has been documented so far. An issue under debate with relevant implications for the seismogenic characterisation of these faults (e.g., earthquake magnitude) is whether these structures die out in the Hormuz salt, or penetrate into the basement, since large earthquakes in the Zagros has been traditionally ascribed to basement faults (e.g., Berberian 1995; Talebian and Jackson, 2004). Better understanding of the strike-slip fault and salt systems, together with earthquake data (e.g., focal depth) can shed light into these practical issues.

This work is focused on the poorly investigated Kareh Bas strike-slip fault and the associated salt extrusions. Based on the integration of new cartographic data, including a general map and a detailed field-based map of a key section (Dandenjan diapir and anticline), together with historical and instrumental earthquake catalogues (Ambraseys and Melville, 1982; Berberian, 2014; Karasözen et al., 2019), we provide some insight into a number of aspects related to the Kareh Bas Fault and the associated salt extrusions: (1) relative chronology of the row of salt extrusions associated with the S-propagating Kareh Bas Fault; (2) mechanical relationship between the Kareh Bas Fault and the Dandenjan Diapir and the role played by the latter on fault segmentation; (3) subsidiary structures associated with the Dandenjan Diapir and the Kareh Bas Fault, including a synorogenic progressive unconformity recording the onset of folding, and the active Dandenjan pull-apart basin; (4) first documented evidence of Quaternary deformation and coseismic surface deformation on the Kareh Bas Fault; (5) potential role played by segmentation and the deep Hormuz salt detachment on the seismogenic potential of the Kareh Bas fault system; and (6) spatial relationship between large, potentially coseismic landslides and the Kareh Bas fault system.

2. Geological setting

2.1. Geotectonic setting

The NW-SE-oriented Zagros Fold and Thrust Belt results from the closure of the Neo-Thetys ocean and the ongoing collision between the Arabian and Eurasian Plates (Fig. 1A). According to GPS data, the Arabian Plate is moving with an orogen-oblique N to NNE direction at a rate of 20–25 mm/yr, of which around one third is accommodated within the Zagros Fold and Thrust Belt (Vernant et al., 2004) (Fig. 1A).

The Zagros Fold and Thrust Belt comprises two principal longitudinal structural domains bounded by the High Zagros Fault; the High Zagros (or Imbricated belt) on the NE, and the Simply Folded Belt on the SW (Fig. 1A). The Main Zagros Reverse Fault defines the NE boundary of the High Zagros, and its northwestern part has been reactivated since the Pliocene as a longitudinal right-lateral strike-slip fault; the so-called Main Recent Fault (Bachmanov et al., 2004; Authemayou et al., 2006). The Simply Folded Belt is divided into three domains with different detachment horizons and structural features, bounded by major oblique N-S and E-W fault zones, from NW to SE (Motiei, 1993; Sepehr and Cosgrove, 2004) (Fig. 1): (1) the Lurestan Arc north of the Balarud Fault; (2) the Dezful Embayment and the Izeh zone; and (3) the Fars Arc east of the right-lateral Kazerun-Borazjan fault system, where this work is focused.

In late Neoproterozoic–early Cambrian times, the ca. 1–1.5 km thick Hormuz salt accumulated in basins controlled by normal faults with a dominant N trend in the SW sector of the Zagros (Kent, 1979; Talbot and Alavi, 1996; Jahani et al., 2017). Subsequently, the region was dominated by sedimentation, largely in shallow marine environments, until the late Cenozoic built up of the Zagros Mountain Belt. The ongoing orogenic phase is essentially recorded by a regressive succession deposited in the Zagros foreland basin overlying the laterally extensive Oligocene-early Miocene Asmari Limestone. It includes the Fars Group (Gachsaran, Mishan and Agha Jari formations, early Miocene-Pliocene) and the continental conglomeratic sediments of the Bakhtyari Formation (Plio-Quaternary) (Motiei, 1993). Growth strata and angular unconformities reveal that the onset of folding occurred at the Eocene-Oligocene transition in the NE of the Simply Folded Belt and propagated progressively to the SW during deposition of the Gachsaran, Mishan and Agha Jari formations (Hessami et al., 2001a). Nonetheless, the basal unconformity of the synorogenic clastics (molasse) of the Bakhtyari Formation is considered to record the onset of significant morphogenetic folding and relief creation in each sector of the Zagros (Hessami et al., 2001a; Mouthereau et al., 2007; Gutiérrez et al., 2023a, 2023b). This is a time-transgressive angular unconformity progressively younger to the SE that cuts across multiple formations. The SW propagation of the collisional deformation implies a progressively younger

age towards the foreland for the onset of a number of processes and their geological record: (1) development of the collision-related structures, including folds, thrusts and S-propagating strike-slip faults; (2) synorogenic clastic sedimentation (e.g., time-transgressive Bakhtyari Formation; Homke et al., 2004; Fakhari et al., 2008; Khadivi et al., 2010; Ruh et al., 2014; Vergés et al., 2019); (3) onset of the squeezing by contractional loading of precursor salt diapirs, eventually leading to salt extrusions (Letouzey and Sherkati, 2004); and (4) initiation of the present-day tectonic landscape dominated by anticlinal ridges and synclinal depressions, as well as longitudinal drainages and some antecedent transverse drainages (Oberlander, 1985; Oveisi et al., 2009; Burberry et al., 2008, 2010; Leturmy et al., 2010;, Mouthereau et al., 2007; Ramsey et al., 2008; Brettis et al., 2011; Collignon et al., 2016; Gutiérrez et al., 2023a; Zarei et al., 2023).

2.2. General features of the Fars Arc

The Fars Arc is characterised by a belt of salt-detachment folds with an overall arcuate arrangement (Fig. 1B). It displays more than one hundred emergent or buried salt diapirs of the Hormuz salt (Jahani et al., 2009, 2017; Gutiérrez et al., 2023b). The distribution of the diapirs is limited to the west by the Kazerun-Borazjan fault system, suggesting that this major structure is inherited from the down-to-the-east normal fault that bounded the Hormuz salt basin in late Neoproterozoic-early Cambrian times (Berberian, 1995; Talbot and Alavi, 1996; Sepehr and Cosgrove, 2004, 2005; Jahani et al., 2017) (Fig. 1B). The curvature of the Fars Arc, which causes an along-strike change to the NW from orthogonal to oblique convergence, plus the greater advance of the deformation in the Fars Arc underlain by thick salt, determines strain partitioning. The deformation is accommodated by shortening across longitudinal folds and reverse faults, plus dextral displacement along a series of oblique N- to NNW-oriented strike-slip faults with associated salt extrusions in the NW limb of the Fars Arc (Berberian, 1995; Hessami et al., 2001b; Talbot and Alavi, 1996; Authemayou et al., 2006; Jahani et al., 2017; Hassanpour et al., 2018) (Fig. 1A).

2.3. Strike-slip faults in the Fars Arc

The western sector of the Fars Arc displays four main N- to NNW-trending right-lateral strike slip fault systems, progressively shorter to the east. These include from W to E (Berberian and Tchalenko, 1976; Berberian, 1995) (Fig. 1B): (1) the Kazerun-Borazjan fault system; (2) the Kerah Bas (or Mengarak) fault system; (3) the Sabz Pushan fault zone; and (4) the Sarvestan Fault. These faults, highly oblique to the NW-SE trend of the shortening structures and nearly parallel to the convergence direction, display the following features (Berberian, 1995; Hessami et al., 2001b; Authemayou et al., 2006, 2009; Faghih et al., 2016; Hassanpour et al., 2018): (1) dextral offset of folds and local deflection of fold axes; (2) alignments of salt extrusions, typically associated with anticlines; (3) several geometric segments, often terminating at their southern end with sharp eastward reverse-fault bends associated with the steeper or overturned southern limb of anticlines; (4) conspicuous geomorphic expression; and (5) ascribable damaging earthquakes.

The N-S-trending Kazerun-Borazjan fault system comprises two main geometrical segments with a right-stepping arrangement and separated by a major stepover (Berberian, 1981, 1995; Jahani et al., 2017) (Fig. 1B). The northern 140 km long Kazerun segment controls the strongly elongated Kamarij salt extrusion (12 km long) and is considered the source of the 1891 (Io VIII) and 1824 (Io VIII; >150 killed in Kazerun) historical earthquakes (Berberian, 1995). A trench excavated in the southern section of the fault (8.5 km N of Kamarij diapir, 39 R 549738.899 E 3289598.017 N) by Bachmanov et al. (2004) exposed folded Quaternary sediments interpreted as coseismic surface bending of unconsolidated deposits. The authors inferred a minimum of two paleoearthquakes younger than 9 ka, with vertical displacement per event of around 1.5 m. Authemayou et al. (2009) estimated maximum long-term horizontal slip rates in the Kazerun segment using lateral offsets of fans and terraces and minimum ages obtained by in situ cosmogenic ^{36}Cl exposure dating on carbonate cobbles sampled on the geomorphic surfaces, assuming no inheritance and no erosion. Rates of $\leq$2.5–4 mm/yr and $\leq$1.5–3.5 mm/yr were calculated for the northern and southern sections of the Kazerun segment. The southern 90 km long Borazjan segment has a significant down-to-the-west throw and controls the Chah Pir and Khormuj salt extrusions, as well as several thermal and sulphur springs (Berberian, 1995) (Fig. 1B). South of the Borazjan Fault segment, the Kuh-e-Namak (or Dashti) diapir occurs associated with a minor right-lateral fault strand. Bachmanov et al. (2004) and Authemayou et al. (2009), based on the limited evidence of lateral offset on geomorphic markers suggested a significantly lower slip rate on the Borazjan segment than on the Kazerun segment.

The Sabz-Pushan fault zone is an ill-defined fault system expressed as local right-lateral offsets and lazy-Z-shaped wrench anticlines with nearby buried salt plugs (Fig. 1B). This structure might have been the source of the M_w 5.6 and 5.8 earthquakes of 1985 and 1987 (Baker et al., 1993; Maggi et al., 2000) and probably also the two M_s~6.4 historical events of 1824 and 1890 (Berberian, 1995). The ca. 100 km long and NNW-oriented Sarvestan Fault controls the location of the Sarvestan, N Kulah-Qazi and S Kulah-Qazi salt extrusions (Fig. 1B). This fault has not generated any damaging earthquake during the instrumental period (from 1900 AD; Berberian, 2014), but was probably the source of the 1890 M_s 6.4 earthquake felt in Fasa town, ca. 12 km east of the fault trace, which killed 30 people (Ambraseys and Melville, 1982; Berberian, 1995, 2014).

GPS measurements indicate that at around 50°E (i.e., western Fars Arc) the Arabian and Eurasian plates converge with a NNE vector at 21 mm/yr, of which 7 $\pm$ 2 mm/yr are accommodated in the Zagros (Vernant et al., 2004; Walpersdorf et al., 2006). Tavakoli et al. (2008), based on measurements from a dedicated GPS network (2-year measurement interval, horizontal velocity uncertainty of $\leq$2 mm/yr), assessed horizontal slip rates along the right-lateral strike slip faults on the western limb of the Fars Arc: (1) 3.6 $\pm$ 0.6 mm/yr on the northern and central sections of the Kazerun fault system; and (2) 3.4 $\pm$ 0.3 mm/yr on the Kerah Bas fault system. In agreement with geomorphic observations (Bachmanov et al., 2004; Authemayou et al., 2009), no significant motion was detected across the Borazjan segment, the Sabz Pushan fault system and the Saverstan Fault. Their data indicate that the Kazerun and Kerah Bas faults accommodate most of the differential motion between the Fars Arc and the Dezful Embayment.

2.4. Seismotectonics

Seismogenic faulting in the Fars Arc is influenced by the rheological profile, comprising from base to top (O'Brien, 1957; Molinaro et al., 2005): (1) the "rigid basement" of the Arabian metamorphic shield; (2) the "lower mobile group" corresponding to the Hormuz salt, with significant primary and secondary thickness variations; (3) the "competent group" up to the top of the Asmari Formation, formed by a succession up to 10 km thick dominated by mechanically resistant carbonates; (4) the "upper mobile group" consisting of evaporitic sediments of the Gachsaran Formation; and (5) the "incompetent group" including the Mishan marls and the Agha Jari marls and sandstones. The two mobile groups and the incompetent group can restrict the propagation of ruptures and prevent the formation of coseismic surface ruptures (Berberian, 1995), limiting the use of paleoseismic methods for seismic source characterisation in hazard analyses.

Traditionally, seismicity in the Fars Arc has been attributed primarily to blind, high-angle reverse faults, and locally to strike-slip faults mostly distributed within the western Fars (Jackson, 1980; Berberian, 1995; Talebian and Jackson, 2004) (Fig. 1B). According to Berberian (1995), the location of the main capable blind reverse faults, such as the inferred

Mountain Front Fault, can be recognized by distinctive anticlines, characterised by: (1) asymmetric geometry with steeper southern limbs; (2) substantial down-to-the south topographic drops and stratigraphic throws; and (3) rare exposures of old formations. In fact, the two reverse fault earthquakes of $M_w \geq 6.7$ occurred in the instrumental period were associated with this type of anticlines and did not produce primary surface ruptures (1972 Ghir, and 1977 Khurgu; Dewey and Grantz, 1973; Berberian and Papastamatiou, 1978; see location in Fig. 1B).

Recent data on locally- and teleseismically-recorded earthquakes, together with rupture depth derived from DInSAR inverted data (e.g., Lohman and Simons, 2005; Roustaei et al., 2010; Barnhart et al., 2013) reveal two main types of reverse fault earthquakes in the Fars Arc (Nissen et al., 2011): (1) Moderate-size events (M_w 5–6, focal depths 5–10 km) produced by non-outcropping faults within the "competent group" above the Hormuz salt, which account for about half of the earthquakes. (2) Infrequent large-size earthquakes ($M_w > 6$, focal depths >10 km), presumably sourced from basement faults and typically associated with the distinctive S-verging asymmetric anticlines of Berberian (1995), that can also rupture through the Hormuz salt and involve the cover. Karasözen et al. (2019), using a multiple-earthquake relocation technique, analysed the distribution of seismicity across the Zagros Belt using ca. 2500 relocated earthquakes (location errors <5 km, focal depth errors <3 km) spanning ca. 70 years of instrumental record (1951–2018), with calibrated focal depth data for ~1000 of them. Fig. 1B shows the distribution of relocated earthquakes of the catalog produced by Karasözen et al. (2019) in the Fars Arc. It shows that around 70% of the strike-slip earthquakes of the Fars Arc (S of the High Zagros Fault) are associated with the Kazerun-Borazjan, Kareh Bas and Sabz Pushan fault systems. Here, strike-slip earthquakes represent around 42% of the events. As shows the plot of calibrated focal depths of earthquakes in the western Fars (67 events between 51°E and 53.5°E), around 85% of the reverse and strike-slip earthquakes are nucleated within the "competent group" above the Hormuz salt (≤12 km). The hypocentral depth of one fifth of the strike-slip earthquakes occur at 22–27 km, well below the base of the Hormuz salt (labelled in Fig. 1B), most of them associated with the Kazerun Fault.

2.5. Salt diapirs in the Fars Arc

Salt extrusions and buried salt plugs are distributed in two zones of the Fars Arc (Kent, 1979; Talbot and Alavi, 1996; Jahani et al., 2009; Gutiérrez et al., 2023b) (Fig. 1B): (1) the western limb of the Fars Arc, where the majority of the diapirs (13 out of 15) occur associated with N- to NNW-trending right-lateral strike slip faults, and (2) the eastern half of the Fars Arc, where diapirs tend to be associated with anticlines and most of them lack any spatial relationship with surface faults. According to Jahani et al. (2017), the lack of salt diapirs in the intervening area can be attributed to thinner Hormuz salt in an intra-basin horst, designated as the Qatar-Fars Arch.

The development of salt walls and stocks of the Zagros started in pre-orogenic times, amidst a flat-lying overburden (i.e., downbuilding), and these precursor salt plugs were rejuvenated during the Cenozoic collisional deformation (i.e., squeezing by contractional loading) (Harrison, 1930; Kent, 1979; Player, 1969; Talbot and Jarvis, 1984; Talbot and Alavi, 1996; Sherkati et al., 2006; Jahani et al., 2007, 2009, 2017; Snidero et al., 2019; Adineh et al., 2023). The precursor salt plugs, which constitute mechanically weak zones that puncture the cover, have functioned as strain localizers and enhancers, controlling the initiation, propagation and geometry of folds and faults (Letouzey and Sherkati, 2004; Callot et al., 2007; Jahani et al., 2007, 2009, 2017). Different evolutionary stages can be identified in the salt diapirs of the Fars Arc on the basis of their geomorphic features, including buried domes, growing salt domes, salt fountains with a summit dome and spreading namakiers, salt droplets, degrading salt domes, and craters with exposed Hormuz sediment or filled with detrital deposits (Jahani et al., 2007, 2009; Talbot and Pohjola, 2009; Mukherjee et al., 2010; De Waele and Gutiérrez, 2022).

3. Methodology

A general map of the Kareh Bas fault system has been produced using satellite images (ESRI World Imagery) and shaded relief models derived from TanDEM-X DEMs (German Aerospace Center, DLR) with a spatial resolution of 12 m (Wessel, 2016). This map includes the trace of the surface faults and the distribution of large landslides, mainly identified in the hillshades and some depicted in available geological maps (GSI, 1996a, 1996b) (Fig. 2). A geological map of the Dandenjan diapir and the anticline associated with the Kareh Bas Fault was produced following a phased approach. Initially, preliminary maps were drafted by the interpretation of: (1) stereoscopic greyscale aerial photographs from 1956 printed at an approximate scale of 1:40,000; (2) shaded relief models derived from TanDEM-X DEMs (12 m resolution); and (3) satellite images from GoogleEarth with spatial resolution better than 2 m. In a subsequent stage, field surveys were conducted to refine the maps and collect data. Field work was carried out with the aid of satellite images uploaded in a tablet with a GPS sensor.

4. The Kareh Bas fault system and the associated salt extrusions and landslides

4.1. Neotectonics of the Kareh Bas fault system

The NNW-SSE-oriented Kareh Bas fault system, with an aggregate length of 220 km, is located 65 km east of the Kazerun-Borazjan fault system and 25 km west of Shiraz city (Fig. 1B). It comprises three geometric segments that connect at their southern terminations with longitudinal ENE-WSW-striking and S-verging reverse faults associated with the southern steeper to overturned limb of anticlines (contractional bend terminations). From N to S the segments include (Fig. 2): (1) the 120 km long Kareh Bas N segment; (2) the 56 km long Kareh Bas S segment; and (3) the 44 km long Kareh Bas SW segment (or Bahar Fault; Jahani et al., 2017). The N and S segments show a left-stepping en echelon arrangement, linked by the Dandenjan reverse fault at the stepover. The S and SW segments display a right-stepping and overlapping distribution and terminate at the Surmeh and Kalagh reverse faults, respectively. The S segment splits into two fault strands between the Konarsiah and Jahani diapirs. Some anticlines offset by the latter two segments host gas fields of the Paleozoic Petrolum System (e.g., Aghar, Dalan; Bordenave and Hegre, 2010).

Two pull-apart basins with conspicuous geomorphic expression occur associated with the Kareh Bas N segment (Fig. 2): (1) the 11.5 km long Kareh Bas Basin associated with the Dalu Anticline and drained by the Rudkhaneh River; and (2) the 11 km long and internally drained Dandenjan Basin, associated with the Dandenjan Anticline. Around 16 km to the NW of the Kareh Bas Basin the Dalu Anticline is truncated by the NNE-SSW-oriented, 20 km long and 6.5 km wide Arjhan Graben, which hosts the Arjhan Lake. This basin is bounded by prominent escarpments up to 300 m high with hanging valleys controlled by NNE-SSW faults that veer into a N-S trend to the south.

The folds are offset by the right-lateral Kareh Bas Fault. This cartographic relationship indicates that fault initiation was coeval or more likely subsequent to the onset of folding (Sepehr and Cosgrove, 2005; Hassanpour et al., 2018). The fault trace coincides with some anticline culminations (e.g., Dalu, Salamati, Dandenjan; Talbot and Alavi, 1996) and the axes of some folds show bends in the vicinity of the fault consistent with ductile dextral shearing. Some laterally offset anticlines lacking significant changes in the trend of their axes and strata across the fault can be used to assess the cumulative horizontal displacement along the Kareh Bas N fault segment, assuming that folds used to extend across the fault and predate faulting (Fig. 2). The axes of the Dalu and Salamati anticlines show horizontal offsets of 4.9 km, 4.4 km, respectively. On the northern limb of the Dandenjan Anticline, the Asmari-Gachsaran contact (unaffected by reverse faulting unlike the southern limb) displays a far-field offset of 5.7 km.

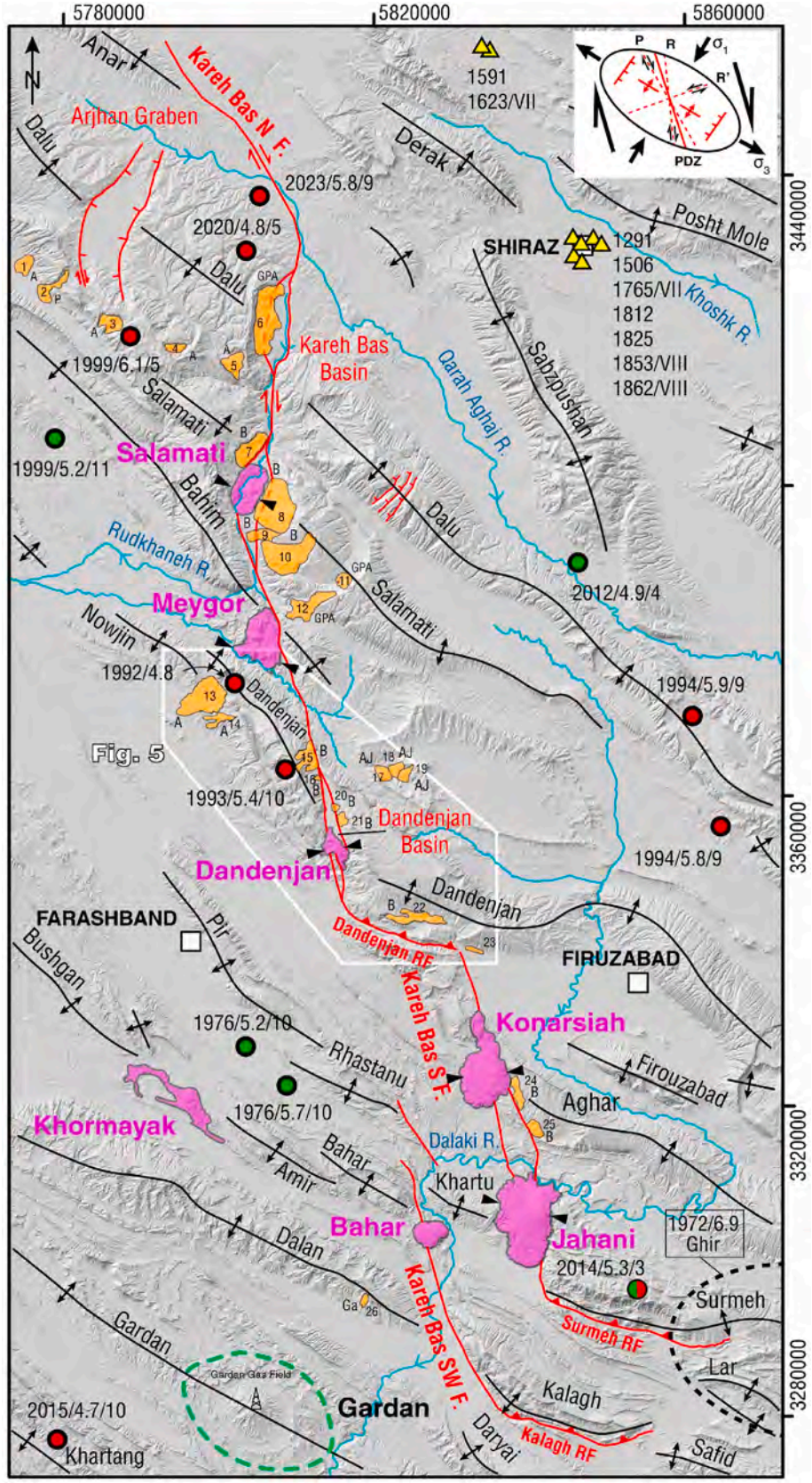

(caption on next page)

Fig. 2. Shaded relief model with the different geometric segments of the Kareh Bas fault system, the associated salt extrusions, the distribution of large landslides (orange polygons) and seismicity. Historical earthquakes from the catalogs (10–1000 AD) of Ambraseys and Melville (1982) and Berberian (2014) are indicated with triangles, together with the year and intensity in the Modified Mercalli scale. Most of the epicentres of the instrumental earthquakes are derived from the relocated earthquake catalog (1951–2018; location error <5 km) of Karasözen et al. (2019), differentiating the dominant style of faulting (red: strike-slip; green: reverse), and indicating their date, magnitude and calibrated focal depth (uncertainty <5 km). Earthquakes younger than 2018 are from the database of the Iranian Seismological Center. No moderate or large earthquakes were recorded in the area between 1990–1951 (Berberian, 2014). The black dashed line depicts the meizoseismal zone of the 1972 M_s 6.9 reverse fault Qir earthquake, with the epicentre located to the east of the map area. See additional data in Table 1. Main stratigraphic units involved in the landslides are indicated with capital letters (B: Bangestan; G: Guri, P: Pabdeh, A: Asmari; Ga: Gachsaran). Triangles indicate the location of the topographic profiles across the salt extrusions shown in Fig. 4. Inset shows strain ellipsoid associated with a NNW-SSE right-lateral strike-slip fault. Green dashed line indicates a buried diapir. (For interpretation of the references to colour in this figure legend, the reader is referred to the Web version of this article.)

Field work conducted in the fault sections around Dandenjan, Konarsiah and Jahani diapirs has allowed us to identify for the first time outcrops of the fault with associated deformed Quaternary deposits. South of Dandenjan Diapir (39R 620838E 3202784N) an exposure located at the apex of an alluvial fan shows a master subvertical fault with down-to-the west displacement juxtaposing Quaternary alluvium against strongly fractured Asmari limestone. The shear zone associated with this fault plane displays large blocks of limestone with rotated fabrics. Secondary faulting with vertical displacement can be observed within the stratified alluvium in the downthrown block (Fig. SP1 in supplementary material). Just N of Bachun village, close to the linkage zone between the strike-slip N segment and Dandenjan reverse fault (39R 621320E 3202086N), an outcrop at the foot of the mountain front displays a steep fault plane with down-to-the-west displacement component that juxtaposes massive bouldery Quaternary colluvial-alluvial deposits with rotated fabrics against steeply dipping to overturned (i.e., drag folded), fractured to brecciated bedrock (Gachsaran, Asmari) (Fig. SP2 in supplementary material).

North of the Jahani salt extrusion the western NNW-oriented strand of the S fault segment has deformed a gravel terrace of the W-flowing Dalaki River, which aggradation surface lies 40 m above the current channel (39R 640468E 3171921N). The exposures on the northern margin of the valley, including the cutting of a dirt road, show a steep fault plane with down-to-the-E displacement component and three packages in the terrace deposits differentiated based on the degree of deformation (Fig. 3). The lower one, restricted to the downthrown upstream block corresponds to faulted gravels with an abrupt downward bend close to the fault. An intermediate package, well exposed in the E-W-oriented road cutting and that extends across the trace of the fault, displays a synformal structure with the following features: (1) the hinge coincides with the trace of the fault; (2) gravel beds on the western limb of the fold clearly dip upstream (apparent dip 5-7 E), indicating that they have been affected by post-sedimentary deformation; (3) the core of the synform is filled by anomalous well-sorted sand facies 2.7–4 m thick, only observable at this specific site. The upper package corresponds to the laterally continuous and non-deformed uppermost unit of the terrace deposit. A similar synform on gravel deposits with sand facies within its core can be also observed associated with the fault on the opposite side of the valley, but with poorer exposure conditions.

The stratigraphic and structural relationships observed at this site allow us to infer a minimum of two surface faulting or folding events occurred during the accumulation of the terrace deposits. The oldest one ruptured the lower gravel package. This event created adequate topographic conditions (e.g., upstream-facing scarp) for the preservation of the gravels in the downthrown block and their erosion from the downstream uplifted side. A younger meter-scale displacement event folded the gravels of the intermediate package, generating a transverse fault-parallel trough subsequently filled by sand facies. Coseismic surface folding created local hydraulic conditions (flow depth increase and velocity drop) that favoured rapid deposition of fine-grained facies, only observable at this site. The fact that the upper gravel package does not show any evidence of deformation suggests that this corresponds to the most recent surface-deforming event on the western strand of the Kareh Bas fault at this site. Geochronological analyses (e.g. Optically Stimulated Luminescence) would allow constraining the timing of the paleoearthquakes. Around 3 km NNW (39R 639714E 3174653N) a plane of the western fault strand (N173E83W) has been exposed by differential erosion. The plane on limestone (Garulizak Member of the Mishan Formation; N173E83 W) at the eastern wall displays striations with a rake of 19S, indicating dextral displacement with some down-to-the-E component, consistent with the terrace outcrop analysed further south (Figs. SP3, SP4 in supplementary material).

4.2. Seismicity associated with the Kareh Bas fault system

Fig. 2 shows the distribution of historically and instrumentally recorded earthquakes within an area of ca. 19,000 km^2 around the Kareh Bas fault system, including Shiraz City, currently with over 1.6 million inhabitants. Some data on those events are included in Table 1. It should be noted that the location of the epicentres of the historical earthquakes is unknown, and that it is practically impossible to assess epicentral intensities greater than VIII for pre-instrumental earthquakes in Iran, because of the weak nature of the constructions, including widespread adobe buildings (Ambraseys and Melville, 1982). Seismicity in the area shows the following general patterns.

(1) All the records of historical damaging earthquakes are restricted to ancient large population centres, including Marvdasht-Persepolis area (1591, 1623) 40 km N of Shiraz, and Shiraz City (1291, 1506, 1765, 1812, 1825, 1953, 1862). The most devastating event was the May 4, 1853 (I_o VIII) Shiraz earthquake, which induced liquefaction and caused 9000–11,000 fatalities as well as almost total destruction of the city (Ambraseys and Melville, 1982; Berberian, 2014).
(2) The M_w 4.8–5.7 earthquakes located at >20 km distance from the Kareh Bas fault system, dated 1976, 1976, 1999, 2012, show a dominant reverse fault mechanism (green circles). These events with focal depths ≤11 km are most likely sourced from blind reverse faults within the supra-salt competent group (Nissen et al., 2011).
(3) Five out of six of the earthquakes spatially associated with the Kareh Bas Fault show dominant strike-slip faulting and focal depths within the 5–10 km range. The 1999, M_w 6.1 Kuhmareh Sorkhi earthquake, located S of the Arjhan Graben, killed and injured 26 and 100 people, respectively, and destroyed 9 villages (Berberian, 2014). The 1992 event NW of Dandenjan Diapir killed one person and destroyed 5 villages, while the nearby 1993 earthquake destroyed 16 villages (Berberian, 2014). The focal solution of this event with 0 rake indicates pure strike-slip faulting (Karasözen et al., 2019). The 2014 M_w 5.3 earthquake located on the Surmeh Anticline and with a focal mechanism indicating mixed reverse-dextral displacement (135 rake; Table 1) can be ascribed to a shallow rupture within the supra-salt cover (3 km focal depth) along the southern termination of the Kareh Bas S fault segment, expressed as a longitudinal reverse fault along the southern limb of the anticline.
(4) Two strike-slip earthquakes N of Firuzabad (M_w 5.8–5.9) with 9 km focal depth can be related to the buried Sabz Pushan right-lateral fault zone (shown in Fig. 1) proposed by Berberian and Tchalenko (1976) on the basis of earthquake data and dextral

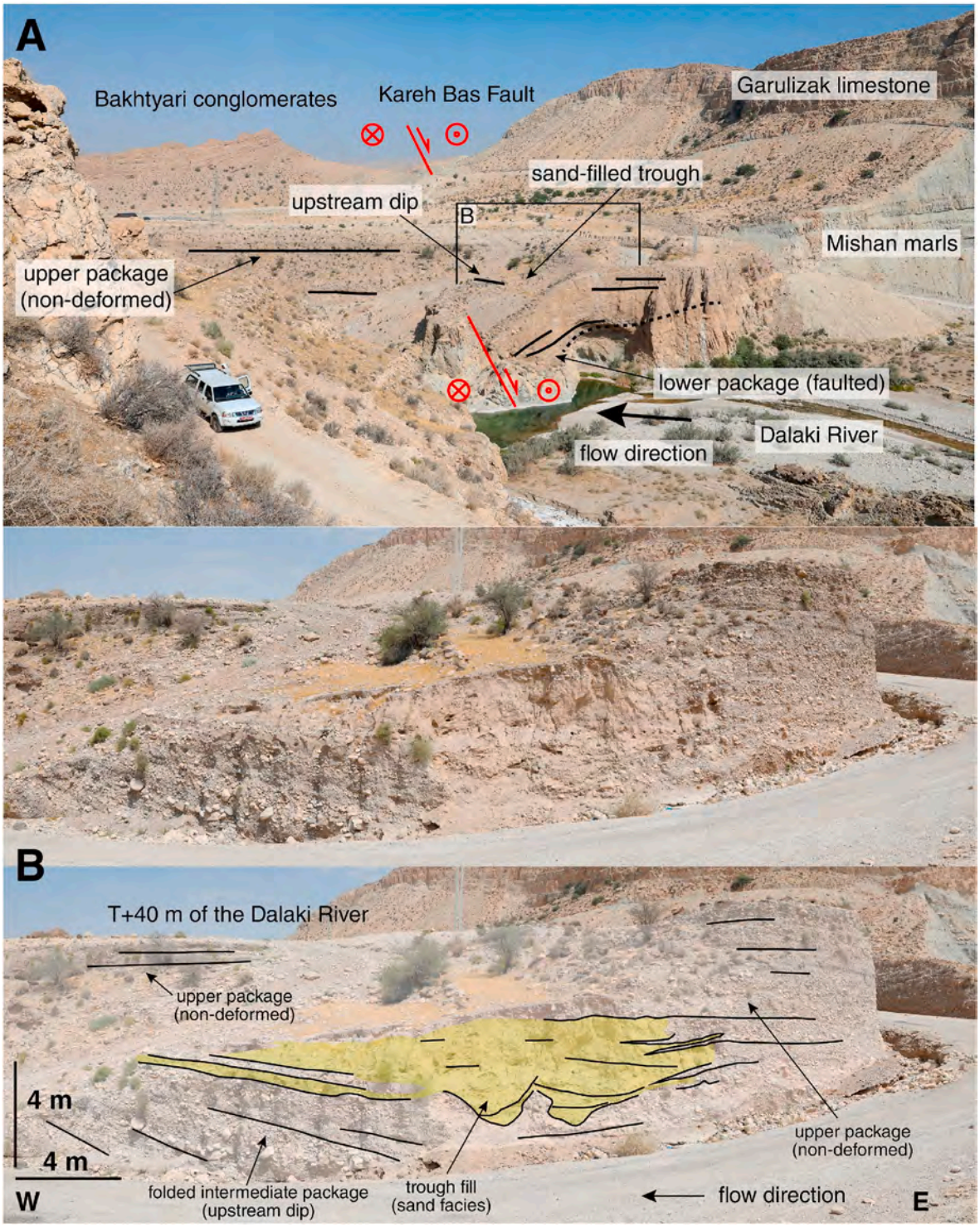

Fig. 3. Terrace of the Dalaki River deformed by episodic displacement on the Kerah Bas. A: Sand-filled trough associated with folded gravels recording the most recent surface-deforming event. Note gravel on the western limb of the synform dipping upstream and non-deformed gravels at the top of the sequence. B: Exposure of the fault with down-to-the-E displacement that offset bent gravels at the base of the terrace deposit. See text for further explanation.

ductile shearing of fold axes. According to Berberian (1995) this NNW-SSE fault zone extends along ca. 120 km from Shiraz to Qir. The 2015 strike slip earthquake on the SW corner of the map is located relatively close to one of the fault strands of the Kazerun strike slip fault.

The epicentre of the Qir (or Ghir) earthquake of April 10, 1972 (M_s 6.9) was associated with the Surmeh Anticline and is traditionally considered as one of the two largest earthquakes generated by blind reverse faults in the seismic history of the Zagros. The earthquake, with a focal depth of 10 km, was generated by a WNW-ESE and N-dipping reverse fault. The source is considered as the eastern prolongation of the exposed WNW-ESE-trending and N-dipping Surmeh reverse fault at the southern termination of the Kareh Bas Fault and associated with the southern overturned limb of the asymmetric Surmeh Anticline (Dewey and Grantz, 1973; Berberian, 1995, 2014; Karasözen et al., 2019). This

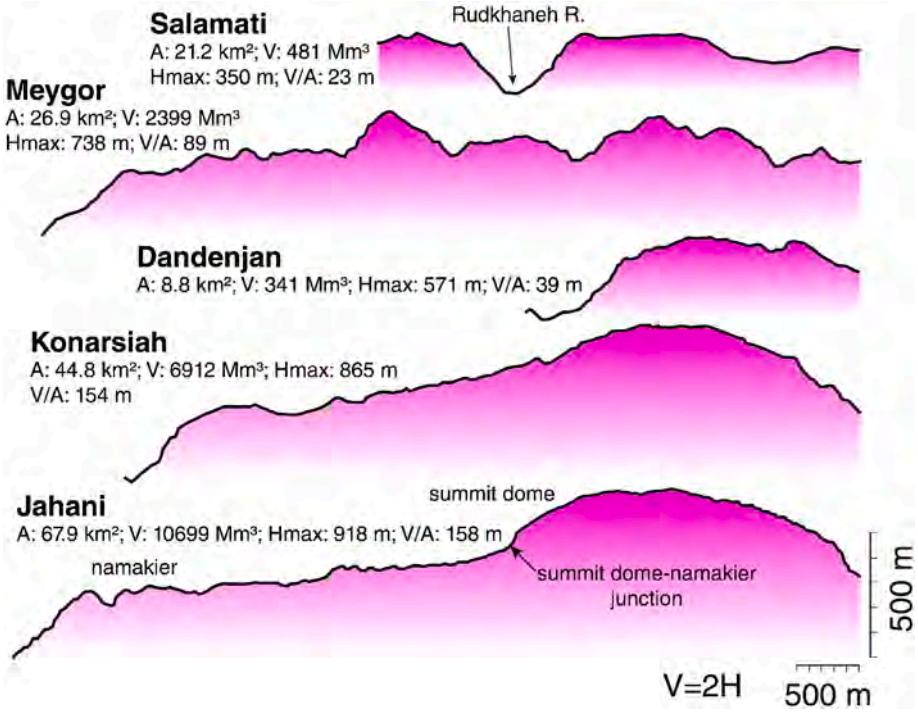

Fig. 4. Transverse topographic profiles (x2 vertical exaggeration) and morphometric parameters of the salt extrusions associated with the Kareh Bas N and S fault segments. A: area; V: volume; Hmax: maximum local relief; V/A: volume to area ratio as measure of average thickness. See location of topographic profiles in Fig. 2.

Table 1
Data of historically and instrumentally recorded earthquakes plotted in Fig. 2. The intensity (I) refers to the Modified Mercalli Scale. The dominant style of faulting indicated with letters; SS: strike-slip; R: reverse. The source of the data is quoted with initials, AM: Ambraseys and Melville (1982); B: Berberian (2014); ISC: Iranian Seismological Center; K: Karasözen et al. (2019).

Date	Coordinates (N-E)	Location	I	M_s	M_w	Style of faulting	Strike	Dip	Rake	Focal depth	Damage	Catalog
1291		Shiraz									Damage on buildings	AM
1506.05.24		Shiraz	>VII								Damage on buildings	AM, B
1591.10.08	29.8–52.4	NW Shiraz	>VII	5.9							Building destruction	AM, B
1623	29.92–52.92	Parsé	>VII	>5.5							Damage in Persepolis, Estakhr, Marvdasht	AM, B
1765.04.23	29.6–52.5	Shiraz	>VII	>5.5							Damage on buildings	AM, B
1812		Shiraz	>VII								Damage on buildings	AM, B
1825		Shiraz	VII								Building destruction	AM, B
1853.05.05	29.6–52.5	Shiraz	VIII	6.2							9000–11,000 killed, extensive destruction, liquefaction	AM, B
1862.12.21	29.5–52.5	Shiraz	VIII	6.2							Building destruction	AM, B
1972.04.10	28.47474–52.85440	Qir (Ghir, Karzin)	VIII-IX	6.9	6.7	R	288	49	99	10	5010 killed, 50 villages destroyed	K, AM, B
1976.04.22	28.74512–52.18108				5.7	R	312	52	80	10		K
1976.04.26	28.77143–52.15302				5.2	R	282	45	90	10		K
1992.09.08	29.13–52.15	Darenjan	VI	4.8							1 killed, 5 villages destroyed	B
1993.01.06	29.06977–52.18436	Darenjan			5.4	SS	248	76	0	10	16 villages destroyed	K. B
1994.03.01	29.11379–52.65524	Mook			5.9	SS	149	75	177	9	2 killed	K, B
1994.06.20	29.00664–52.67926	Ebhahimabad			5.8	SS	255	74	−3	9	3 killed, 12 villages destroyed	K, B
1999.05.06	29.50910–51.99988	Kuhmareh Sorkhi			6.1	SS	49	77	−12	5	26 killed, 9 villages destroyed	K, B
1999.10.31	29.41309–51.90546				5.2	R	117	34	67	11		K
2012.10.10	29.28302–52.51116				4.9	R	93	47	57	4		K
2014.10.28	28.53776–52.58925				5.0	R/SS	325	53	135	3		K
2015.04.10	28.38573–51.91812				4.7	SS	330	67	174	10		K
2020.01.28	29.59–52.13	Khanehzeniyan			5.8	SS	150	87	−178	5		ISC
2023.01.28	38.59–44.9	Khanehzeniyan			4.8	SS	214	70	−6	9		ISC

reverse fault affects Pliocene Bakhtiari conglomerates and the Surmeh Anticline. According to Berberian (1995) this is the only locality within the Simply Folded Belt where lower Paleozoic rocks are exposed, supporting the presence of a large-throw basement reverse fault. The Qir (or Ghir) earthquake killed more than 5010 people and injured 1400 in a sparsely populated area with around 28,800 residents, and destroyed 50

villages. Reported environmental effects include secondary surface ruptures, liquefaction and occurrence of springs (Dewey and Grantz, 1973; Ambraseys and Melville, 1982; Berberian 1995, 2014; Ambraseys and Jackson, 1998). Berberian (2014) suggests that the longitudinal ground ruptures developed in the hanging wall of the Surmeh reverse fault could correspond to flexural-slip faults.

4.3. Salt extrusions associated with the Kareh Bas fault system

Six salt extrusions (purple polygons in Fig. 2) are distributed along the Kareh Bas fault system, from N to S: Salamati, Meygor and Dandenjan on the N segment, Konarsiah, and Jahani on the S segment, and Bahar on the SW segment. Salamati is associated with a double releasing bend (Cunningham and Mann, 2007; Jackson and Hudec, 2017; Jahani et al., 2017). All the salt extrusions show a clear spatial relationship with laterally offset anticlines, either at the medial sector or at a periclinal termination (e.g., Bahar). The five salt extrusions associated with the Kareh Bas N and S segments display a rather regular spacing between centroids ranging between 17 and 30 km, with an average value of 22.3 km. The morphology of these salt extrusions display a N-to-S gradation in their evolutionary stage, from a highly degraded dome to a vigorously rising salt fountain (Fig. 4). Salamati is a deflated, low-relief salt dome deeply incised along its axis by the Rudkhaneh River. Meygor, with a dominant fluvial landscape, is dissected by a dense drainage network. Dandenjan displays a less dissected and more rounded topography than Meygor. Salamati, Meygor and Dandenjan lack any significant salt exposure. Konarsiah (Zarei et al., 2012) and Jahani (Abirifard et al., 2017) are large salt fountains with widespread salt exposures and extensive salt glaciers riddled by densely packed sinkholes (polygonal karst landscape). Jahani salt extrusion has a well-defined summit dome with a clear concavity and slope break at the dome-namakier junction indicating vigorously rising salt (Fig. 4). In contrast, the summit dome of Konarsiah is rather subdued, suggesting that the salt fountain is transitioning towards a salt droplet. Bahar, associated with the Kareh Bas SW segment is a growing dome largely confined by surrounding reliefs.

The N-S gradation is also supported by some morphometric data extracted from the TanDEM-X DEMs (12 m resolution) (Fig. 4). The maximum local relief corresponds to the elevation difference between the highest point of the extrusion and the lowest point of the perimeter. The volume has been estimated computing the volume of the 3D space enclosed by two TIN surfaces; the topography of the salt extrusion and a basal surface interpolated from the perimeter of the extrusion. This approach may lead to overestimations for the salt fountains but can be used for comparative purposes. The maximum local relief of Salamati, Dandenjan, Konarsiah and Jahani are 350, 571, 865, and 918 m, respectively. The high relief of Meygor (Hmax: 738 m), despite its high degree of dissection, is related to the presence of prominent ridges in the northern sector underlain by thick and laterally continuous black limestones and tan sandstones of the Hormuz Group. A N-S increasing trend is also observed for the volume/area ratio, which is an approximation for the average thickness of emerged salt; 23 m, 39 m, 154 m, 158 m for Salamati, Dandenjan, Konarsiah and Jahani, respectively. Meygor with 89 m is an exception for the reason indicated above.

4.4. Landslide distribution

A total of 26 large bedrock landslides or landslide complexes have been mapped in an area of ca. 19,000 km^2 around the Kareh Bas fault system (labelled in Fig. 2). These slope movements are larger than 0.5 km^2 (6.2 km^2 average) and can reach up to 25 km^2 in cartographic extent (i.e., landslides SE of Salamati). They include multiple types such as slides (3, 4, 5, 6,7, 8, 9, 11,17, 18, 19, 20, 21,24,25, 26), slide-flows (2, 10, 15, 16), translational slides that have produced buckle folds (22, 23), and catastrophic long runout rock avalanches (1, 12, 13, 14). The distribution of the inventoried landslides shows a much higher spatial frequency in the vicinity of the Kareh Bas fault system. The proportion of landslides located at distances from the fault trace equal or smaller than 5 and 10 km are 57.7% and 88.5%, respectively. The number of landslides within the 10–25 km distance range drops to 1 (3.8%).

5. The Dandenjan fault and salt system

5.1. The Dandenjan Anticline and its extensional structures

The following bedrock cartographic units have been differentiated in the mapped area of Dandenjan Anticline (Fig. 5): (1) the Neoproterozoic-Cambrian age Hormuz Group, consisting of white and purple marls and shales, gypsum/anhydrite, black limestone and concealed salt; (2) Early Cretaceous rocks of the Khami Group comprising the Fahlyan Fm. (limestone), the Gadvan Fm. (shales) and the Dariyan Fm. (limestone); (3) the Cretaceous Bangestan Group, including marls and shales of the Kazhdumi Fm. overlain by the Sarvak Limestone Fm.; (4) Late Cretaceous marls of the Gurpi Fm. and Paleogene shales of the Pabdeh Fm.; (5) the ridge-forming Oligocene-Early Miocene Asmari Limestone; (6) marls, limestone and gypsum of the Miocene Gachsaran Fm.; (6) the Miocene age Mishan Fm. consisting of limestone of the Guri Mb., the main intermediate greenish marl unit and the top Garulizak Limestone Mb.; (7) Mio-Pliocene marls and sandstones of the Agha Jari Fm.; and (8) the unconformable Plio-Quaternary conglomerates of the Bakhtyari Fm.

The 130 km long Dandenjan Anticline has a sinuous trace comprising from E to W (Fig. 1B and 2): (1) a NW-trending section with a sharp inflection associated with the Narou buried salt diapir E of Firuzabad; (2) an E-W-oriented section N of Firuzabad; and (3) the WNW-ESE-to NW-SE-western section, where the trend of the fold axis shows a change from N110E to N150E associated with the Kareh Bas Fault and the Dandenjan Diapir. The Dandenjan Anticline and the Salamati Anticline to the N show significant local widenings E of the Salamati and Dandenjan diapirs, respectively (Fig. 2). The Dandenjan Anticline displays contrasting features at both sides of the Kareh Bas Fault, here designated as Dandenjan W and Dandenjan E anticlines (Fig. 5).

The SE-plunging Dandenjan E Anticline on the hanging wall of the Dandenjan reverse fault (southern bend termination of the Kareh Bas N segment) has an asymmetric geometry with a steeper and locally overturned southern limb (Fig. 5). It is twice as wide as the Dandenjan W Anticline. The contrasting wavelength of the buckle fold suggests a thicker supra-salt stratigraphic succession E of the Kareh Bas Fault and the Dandenjan Diapir, probably related to the development of a pre-shortening salt-escape minibasin (Hassanpour et al., 2018). The Dandenjan E Anticline displays a longitudinal graben with geomorphic expression along the hinge zone between the crest and NE limb of the fold. This morphostructure can be ascribed to outer arc extension related to buckle folding. A striking collapse sinkhole occurs on Bangestan limestone associated with the northern uphill-facing scarp of the graben. The anticline is also affected by transverse down-to-the-NW normal faults expressed as conspicuous scarps, ascribable to fold-normal extension in the plunging nose of the anticline.

The NW-plunging Dandenjan W Anticline is significantly narrower, strongly asymmetric and exhibits significant along-strike geometrical variability (Fig. 5). The SW limb, along a section around 8 km long associated with the Kareh Bas Fault and the Dandenjan Diapir, displays a progressive unconformity (i.e., growth strata) (Fig. 6). The apparently conformable strata of Bangestan, Gurpi-Pabdeh and Asmari are overturned. The dip of the Gachsaran Formation changes progressively from around 20°NE in the overturned base of the succession to 50°SW in the non-reversed top. This progressive unconformity with a cumulative rotation of around 70° records deformation coeval with deposition of Gachsaran Formation in the Miocene. Further NW the stratigraphic succession in the SW limb apparently lacks a progressive unconformity and displays a persistent normal SW dipping attitude.

The NE limb, the crest and part of the SW limb of the Dandenjan W Anticline are downthrown mainly by displacement along two down-to-

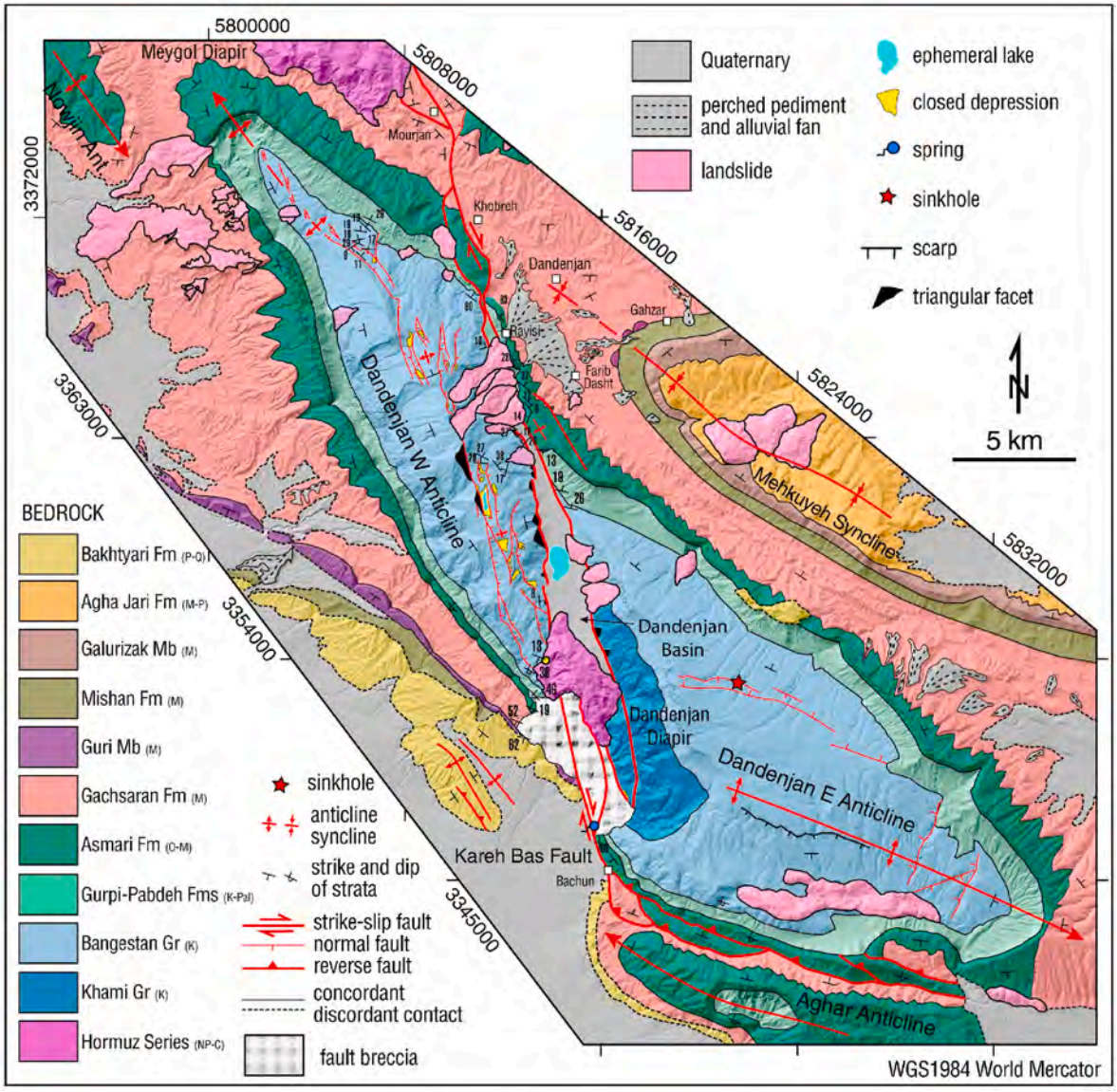

Fig. 5. Geological map of the Dandenjan Anticline and the Dandenjan salt extrusion, both offset by the right-lateral Kareh Bas Fault, with the associated Dandenjan pull-apart basin. See location of mapped area in Fig. 2.

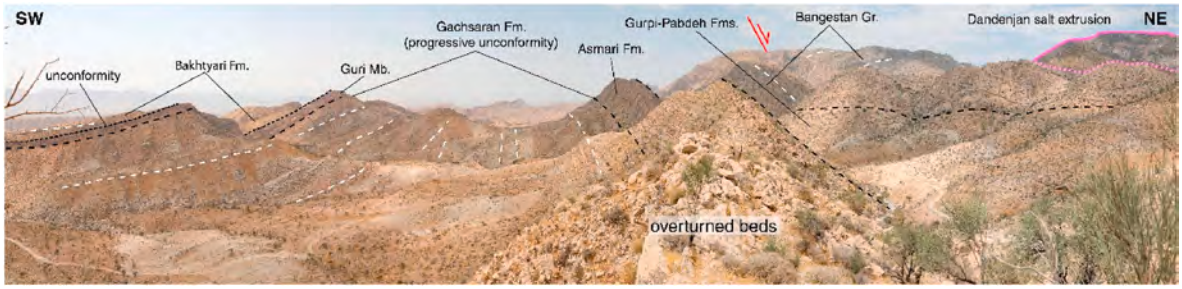

Fig. 6. Progressive unconformity in Gachsaran Formation on the SW limb of the Dandenjan W Anticline, showing a progressive change in the dip of the strata, from overturned (ca. 20NE) to normal (ca. 50SW).

the-NE normal faults with left-stepping and overlapping arrangement (Fig. 5). The 11 km long northern fault, parallel to the fold axis, cuts the SW limb and has downdropped the crest and NE limb of the anticline. The throw of this fault shows an overall decrease towards the NW and dies out within outcrops of the brittle Bangestan Group. This fault is expressed as a NE-facing escarpment with a linear depression along its foot. The structure associated with the depression changes from NW to SE from a rollover anticline (Fig. 7a) to a mixed one showing a rollover anticline offset by an antithetic fault forming a keystone graben (Fig. 7b). The maximum local relief of 190 m of the escarpment associated with the master fault can be considered as a minimum estimate for the vertical offset (i.e., erosion in the footwall and aggradation in the

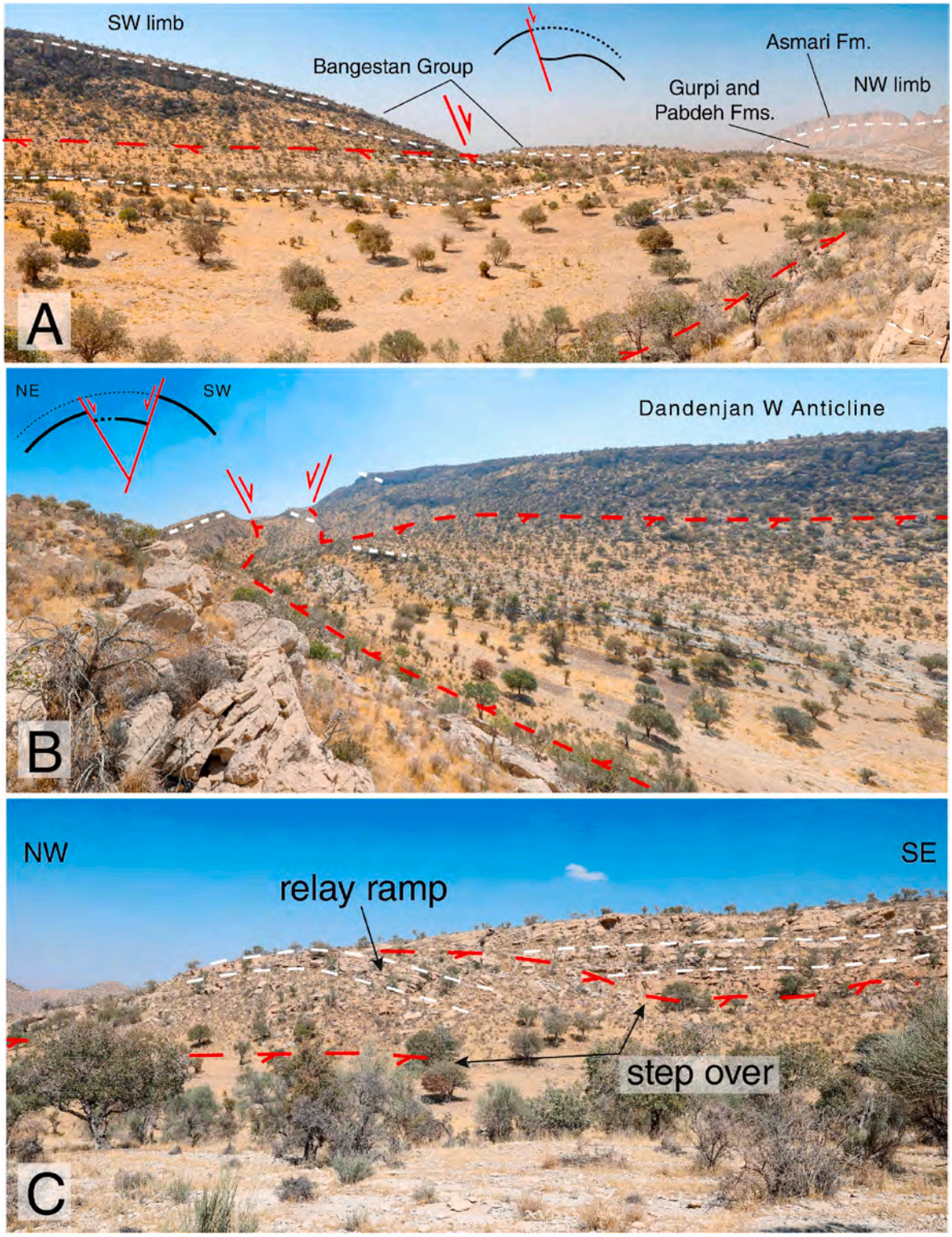

Fig. 7. Northern normal fault in the Dandenjan W Anticline and associated graben. A: Rollover anticline in downthrown block. B: Rollover anticline offset by an antithetic fault forming a keystone graben. C: Soft-linked stepover with relay ramp on the NE margin of the graben.

hanging wall). Locally, the secondary antithetic faults on the NE margin of the graben display well-expressed soft-linked stepovers with relay ramps (Fig. 7c). In the overlapping zone between the northern and southern normal faults there are elongated closed depressions attributable to the headwaters of SW-flowing streams defeated by NE-facing fault scarps (i.e., beheaded drainages) (Fig. 5). The downthrown crest of the Dandenjan W Anticline occurs between the trace of the two main overlapping faults.

The 14.5 km long southern normal fault is slightly oblique with respect to the fold axis, with a more northern trend parallel to the Kareh Bas Fault, and traversing the hinge of the fold in the central section (Fig. 5). This oblique trend determines that the downthrown block affects the NE limb in the northern sector, the crest and NE limb in the central section, and the SW limb, crest and part of the overturned NE

limb in the southern portion. This main southern normal fault is expressed as an E-facing escarpment with two major triangular facets 125 m and 260 m high in the central section. At the foot of the southern facet there is an enclosed keystone graben depression 1 km long that hosts a high-elevation ephemeral lake lying at 2295 m a.s.l. (Fig. 8A). The downthrown side of the main southern fault displays an overall stepped topography dropping towards the Dandenjan pull-apart basin and related to a number of synthetic faults with the following features: (1) short length; (2) common arcuate trace with E-facing concavity; and (3) backtilted downthrown blocks some with sediment-filled asymmetric graben depressions (Fig. 8B). In the southern section the fault splays into several right-stepping fault strands. The western fault strand on the SW limb of the Dandenjan W Anticline juxtaposes normal dipping strata in the hanging wall against overturned beds in the footwall, and its southern termination is associated with the SW edge of the Dandenjan salt extrusion (Fig. 9).

5.2. The Dandenjan pull-apart basin and salt extrusion

The NNW-SSE-striking Kareh Bas Fault dextrally offsets the Dandenjan Anticline showing a short-separation right-releasing stepover associated with the Dandejan salt extrusion and pull-apart basin (Fig. 5). The northern master fault controls the eastern margin of the Dandenjan pull-apart basin, whereas the southern one connects with the Dandenjan reverse fault and is linked to the north, beyond the Dandenjan salt extrusion, with the faults along the western boundary of the pull-apart basin. On the northern limb of the anticline the Kareh Bas Fault displays a horse of strongly fractured Asmari Limestone, expressed as a hill with rounded and subdued topography that contrasts with the typical sharp-crested hogbacks developed on this rock unit. West and south of Rayisi village the fault runs along the Gurpi and Pabdeh formations, but its cartographic trace along a 3.6 km long section is largely buried by a cluster of adjoining landslides. South of the landslide complex two fault strands bound the 11 km long and 1.8 km wide Dandenjan pull-apart basin. This is an enclosed basin characterised by (Figs. 5 and 10): (1)

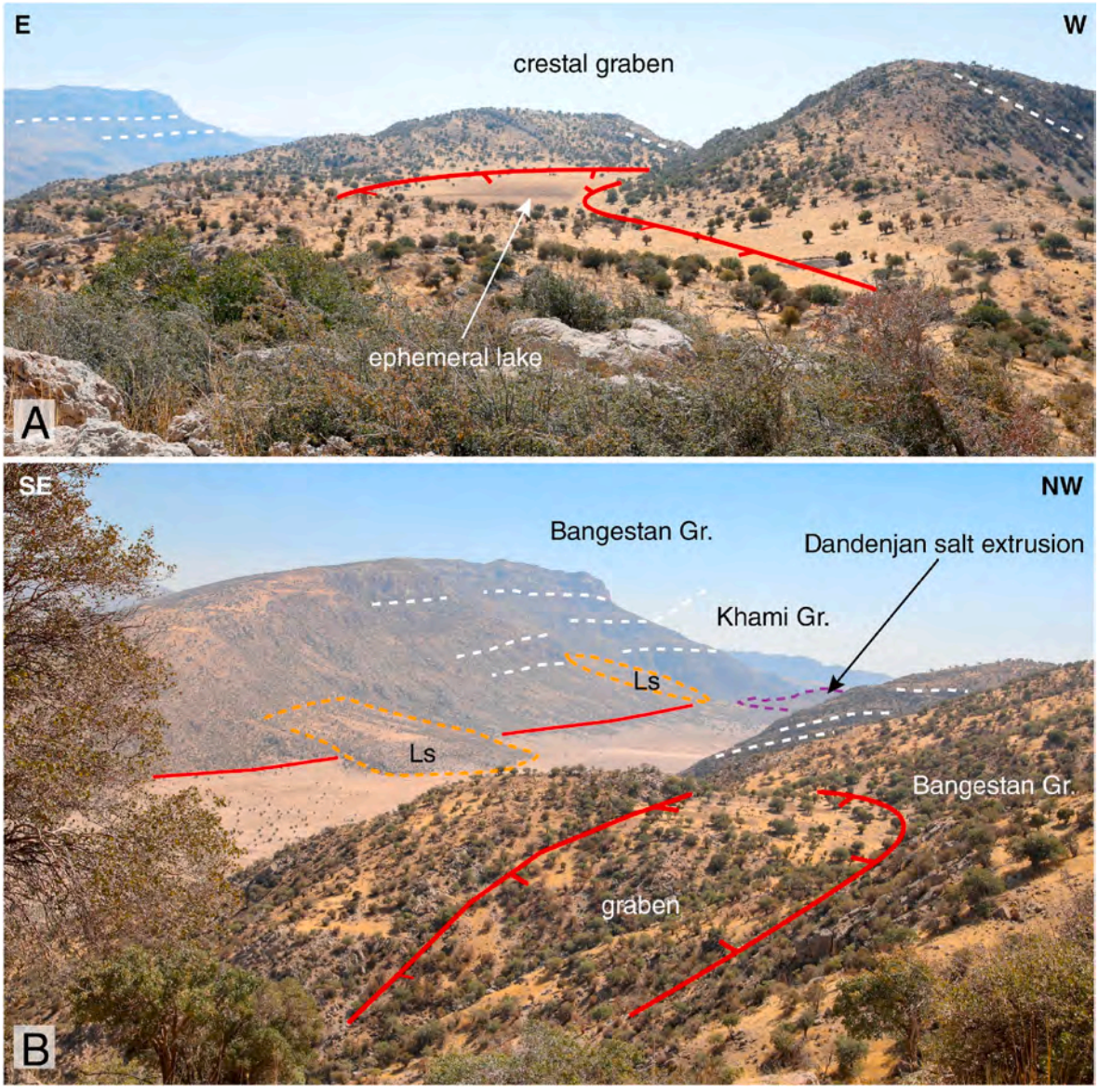

Fig. 8. Extensional morphostructures associated with the southern normal fault in the Dandenjan W Anticline. A: Enclosed depression with an ephemeral lake in a crestal keystone graben. Slope on the right corresponds to a triangular facet 125 m high. B: Secondary graben bounded by a synthetic (right) and antithetic fault (left). In the background the flat floor of the Dandenjan pull-apart basin is locally interrupted by landslides. Note downward bent strata at the margin of the pull-apart basin.

Fig. 9. Normal fault on the SW limb of the Dandenjan Anticline juxtaposing normal dipping strata in the downthrown wall against overturned beds in the footwall. Sketch illustrates general geometrical relationships.

northward-tapering triangular geometry in plan with high elongation ratio (length/width = 6.1); (2) prominent flanking escarpments with triangular facets, indicating significant dip-slip displacement component on the basin-bounding faults; (3) flat aggradational floor with a 1.5 km long ephemeral lake in the central sector lying at 1773 m a.s.l.; and (4) the southern termination, where the basin is widest, is defined by the prominent Dandenjan salt extrusion rising 230 m above the basin floor (Fig. 10B). The basin is bounded on the western margin by a right-stepping array of faults that offset Bangestan limestone. Here, the strata are bent downwards towards the fault (Fig. 10) and grade to fault breccias close to the mountain front-piedmont junction. The rock units offset along the eastern margin include the Khami and Bangestan groups, the Gurpi and Pabdeh formations and the Asmari Limestone, the latter displaying south of Rayisi village strata bent towards the basin forming a secondary anticline (Fig. 5).

The Dandenjan salt extrusion reaches a maximum elevation of 2021 m a.s.l. and shows an elongated geometry in plan, with an aspect ratio of 0.5 (5.8 km long and 3 km wide). Its southern edge shows a right-lateral offset of 2.4 km by a cross fault situated between the master right-stepping faults. The exposure of the fault displays a nearly vertical plane that juxtaposes NW dipping Bangestan limestone against Hormuz sediments (Fig. 11). South of the diapir there is a 2 km wide zone where the bedrock is intensely fractured and brecciated, making difficult to differentiate the rock formations and measure the attitude of the

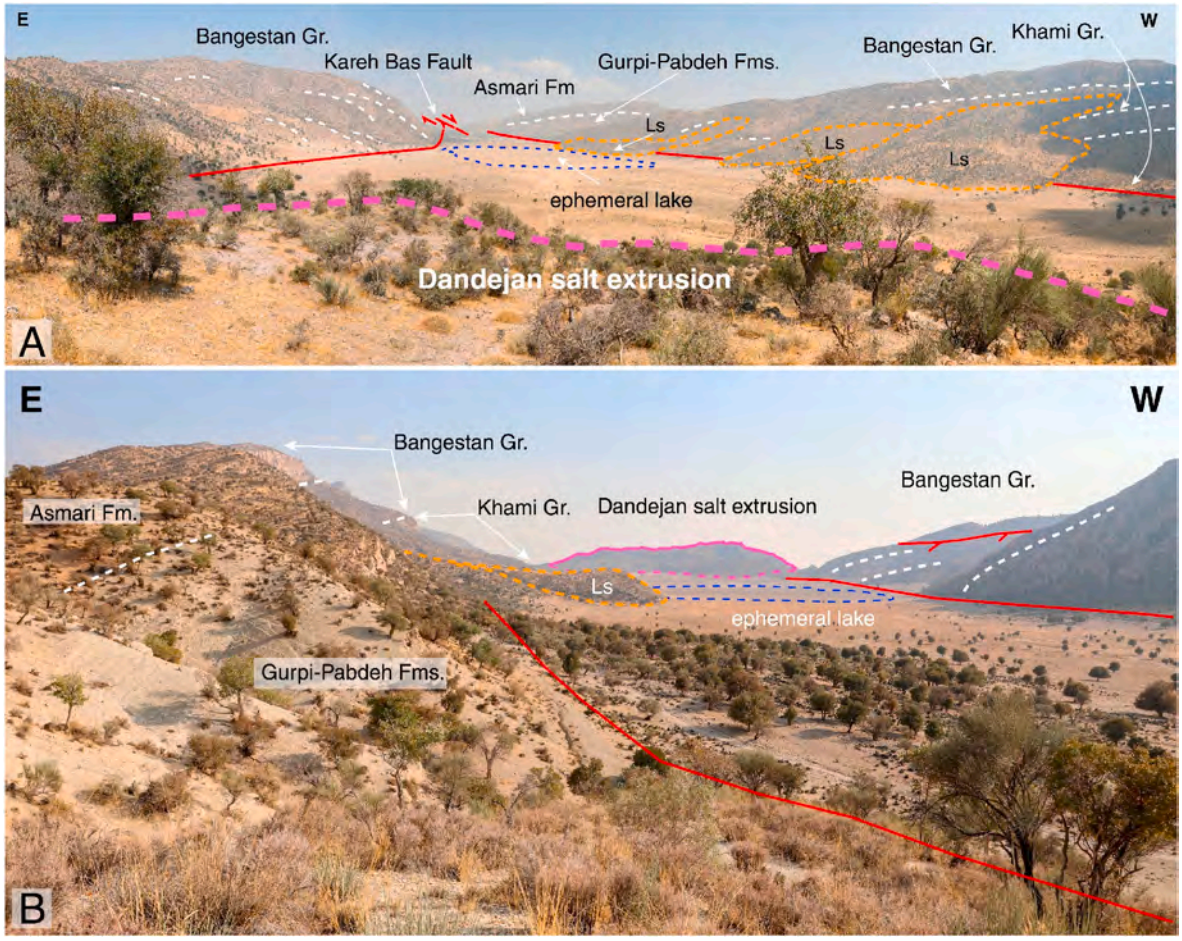

Fig. 10. The Dandenjan pull-apart basin. A: View of the basin looking north showing downward bent Bangestan limestone associated with the western mountain front, the flat floor of the basin with an ephemeral lake, and landslides sourced from different rock formations on the eastern margin. B: View of the basin looking south, with the Dandejan salt extrusion in the background, bent Bangestan limestone on the western margin and a landslide on the eastern side interrupting the flat floor of the basin.

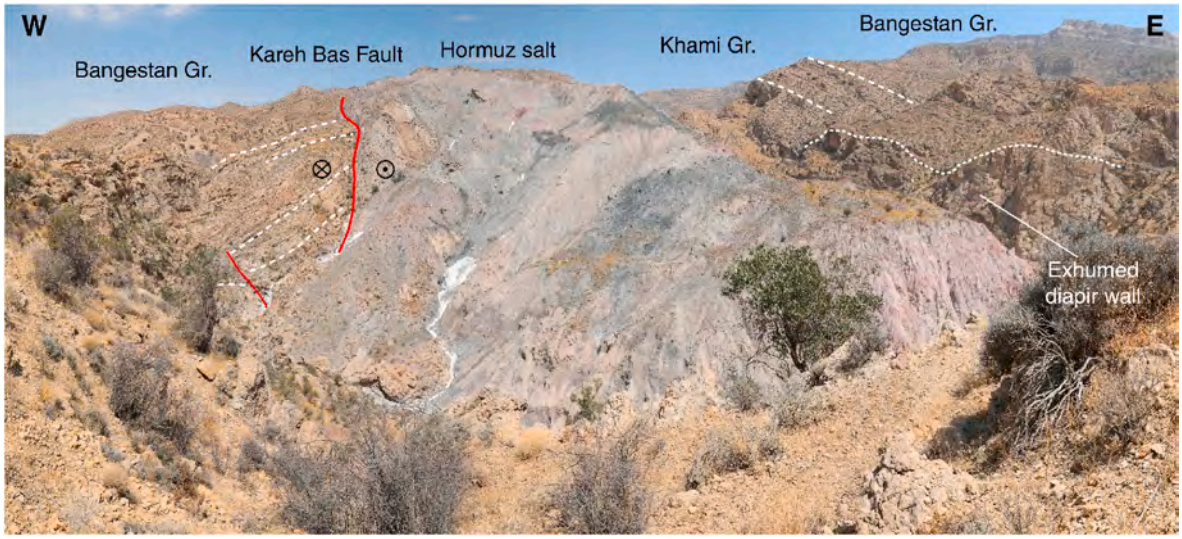

Fig. 11. Southeastern edge of the Dandejan salt extrusion offset dextrally by the Kareh Bas Fault. Note the high proportion of marls and shales in the Hormuz Group with badlands landscape.

bedding (Fig. 5; supplementary material Fig. SP5). In the vicinity of Bachun village there is a major karst spring associated with the Kareh Bas Fault that supplies water to the village and large palm tree plantation. Most probably the fault functions as a hydrogeological barrier controlling the outlet of the aquifer.

5.3. Landslides in the Dandenjan Anticline

A significant number of large landslides (>1 Mm^3) have been mapped in the section of the Dandenjan Anticline associated with the Kareh Bas Fault (Fig. 5). These landslides tend to form spatial clusters. On the SW limb of the Dandenjan W Anticline, next to its NW pericline, two rock avalanches were sourced from a dip slope and ridge of Asmari Limestone, most probably initiated as bedding-controlled planar rock slides (labelled as RA1 and RA2 in Fig. 12). The source of the two rock avalanches is expressed as gaps in the Asmari ridge. Their relative chronology can be established on the basis of several relationships and features: (1) the deposits of RA2 locally onlap those of RA1; (2) RA1 occurs at overall higher relative elevation, and its strongly cemented deposits have functioned as the perched caprock of a mesa-like relief; (3) the fragmentary remains of RA1 are more dissected and degraded. The deposits of RA2 cover a significantly larger area (ca. 20.8 km^2) and display a stepped topography indicating that they were deposited on an irregular surface carved on SW-dipping strata of the Gachsaran Fm., including lithologies with variable resistance to erosion. This rock avalanche, which was laterally confined by the Mowjin anticlinal ridge, shows a runout (L) of 7 km and the maximum vertical drop (H) can be estimated at around 800-700 m, considering the elevation of the ridge in the vicinity of the landslide scar. These figures yield a very low apparent friction coefficient (H/L) of 0.09–0.11 indicating a very high mobility (Scheidegger, 1973). The deposit of the rock avalanche consists of massive, angular, unsorted and chaotic bouldery gravel with a cemented fine-grained matrix, mostly with clast-supported texture (packbreccia; see inset of Fig. 12). This rock avalanche should be older than the Emad Deh rock avalanche of the central Fars Arc, also sourced from a ridge of Asmari limestone, which was dated at 5.4 ka, but with very limited cementation (Gutiérrez et al., 2023a).

On the NE limb of the Dandenjan W Anticline, south of Rayisi village, there is a cluster of six adjoining landslides with an aggregate area of 7.1 km^2. These are rock slides transformed into earth flows up to 3.3 km long developed on a dip slope with a local relief of around 900 m. The landslide deposits consist of massive, chaotic bouldery packbreccias and floatbreccias locally with abundant secondary carbonate (supplementary material Fig. SP6). Several conditioning and preparatory factors

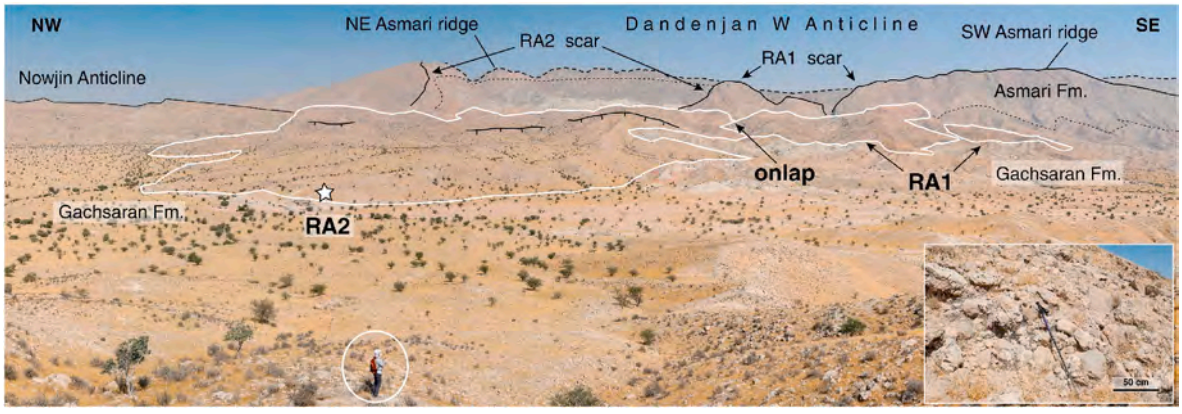

Fig. 12. General view of rock avalanches RA1 and RA2 associated with the SW limb of the Dandenjan W Anticline. The source of the slope failures is expressed as gaps in the Asmari ridge and the deposit of RA2 locally onlaps that of RA1. RA2 shows a stepped topography with downhill-facing scarps indicating that it was deposited on an irregular erosional surface carved in the Gachsaran Fm. Inset shows an image of the deposit of RA2 at the site labelled with a star. It consists of a massive and unsorted packbreccia with a cemented matrix of pulverized fine-grained material.

have favoured the development of these slope movements including: (1) the presence of release planes and weakness zones in the headscar of the landslides corresponding to the synthetic normal faults responsible for the downthrown of the NE limb of the anticline; (2) a stratigraphic succession dipping downslope consisting of resistant Sarvak limestone underlain by mechanically weak marls and shales of the Kazhdumi Fm.; (3) former fluvial downcutting at the foot of the slope guided by the Kareh Bas Fault and easily erodible Gurpi-Pabdeh marls and shales. Both the strike drainage and the fault have been buried by the landslides, some of which were distally confined by a ridge on Asmari limestone, partially surmounted by the slope movements (Fig. 13).

On the east margin of the Dandenjan pull-apart basin there is another cluster of three landslides with an aggregate area of 2.7 km^2 that bury the basin-bounding fault. These are rotational landslides with curved failure planes cut across strata dipping into the slope (Khami and Bangestan groups). At the foot of a dip slope on the southern limb of the Dandenjan E Anticline there is a longitudinal ridge 8.3 km long and covering 2.7 km^2 corresponding to a detachment anticline on strongly fractured limestone. We interpret this apparent parasitic fold (rabbit-ear structure of Hassanpour et al., 2018) as a bedding-controlled translational slide pinned along the foot of the slope in which gravitational gliding is accommodated by shallow detachment folding. The sliding surface was likely controlled by weak marls and shales of the Kazhdumi Fm. underlying the Sarvak limestone (Ghazipour and Simpson, 2017). This interpretation is supported by the presence of a linear scar at higher elevation in the slope. Perry et al. (1965) mapped these feature as a much larger landslide deposit including also the fault breccia south of the Dandenjan salt extrusion. Similar gravitational slope deformations have been documented in other sectors of the Fars Arc (Molinaro et al., 2005; Gutiérrez et al., 2023a).

6. Discussion

6.1. The strike-slip fault and salt diapir system

An evolutionary model for the Kareh Bas-Dandenjan fault-diapir system is proposed based on our detailed geological mapping, together with recent knowledge on the structure of the Fars Arc (Jahani et al., 2009, 2017; Hassanpour et al., 2018), and experience gained by analogue models on the development strike-slip fault zones (Dooley and Schreurs, 2012 and references therein) (Fig. 14). According to Jahani et al. (2017), thicker Hormuz salt (late Neoproterozoic-early Cambrian) was deposited in the hanging wall of N- and NNW-trending, down--to-the-E normal faults in the western Fars Arc. Subsequently, rows of precursor salt walls and stocks developed since the early Paleozoic associated with the infra-salt normal faults. Long-sustained salt rise resulted in a thin and weak supra-salt cover, locally flanked by thickened cover in salt-withdrawal zones (i.e., minibasins of Hassanpour et al., 2018). This could be the case of a pre-shortening Dandenjan Diapir associated with a NNW-oriented basement fault and locally flanked by thicker cover above a salt escape zone (Fig. 14A). During the Cenozoic orogenic phase, the development of collision-related structures (buckle folds, strike-slip faults) propagated to the S within a context of oblique N-to-NE-directed convergence (Vernant et al., 2004). The progressive unconformity observed in the Miocene Gachsaran Formation on the SE limb of the anticline, next to the Dandenjan Diapir, records sedimentation coeval to the initial growth of the anticline (Fig. 6). Most probably the presence of a buried precursor salt plug functioned as a strain localizer and enhancer, controlling the inception of the detachment fold (Letouzey and Sherkati, 2004; Callot et al., 2007; Jahani et al., 2007, 2009, 2017). The timing inferred for the onset of folding at Dandenjan is consistent with observations made by Hessami et al. (2001a), that document basal onlaps and growth strata in the Gachsaran Formation on the northern limb of Aghar and Surmeh anticlines, around 30–50 km to the S (Fig. 2). Hassanpour et al. (2018) interpreted the growth stratal geometry in the Gachsaran Formation as a pre-shortening hook halokinetic sequence recording deposition during the growth of the Dandenjan Diapir. However, the strike of the strata is highly oblique with respect to the edge of the Dandenjan Diapir, the progressive unconformity extends for more than 8 km (Fig. 5), and the Gachsaran Formation was not accumulated next to and atop an emergent diapir, but over a thick supra-salt sedimentary succession (Rowan et al., 2003) (Fig. 6).

The anticline progressively increased its amplitude and propagated laterally. The local widening of the anticline east of the Dandenjan Diapir (i.e., larger wavelength) can be attributed to thicker overburden in a former salt-withdrawal area (Figs. 2 and 14C). A similar situation is found east of Salamati Diapir (Fig. 2). The sharp changes in the direction of the Dandenjan Anticline axis can be related to deflections in the fold propagation path controlled by precursor diapirs (Narou buried diapir E of Firuzabad; Fig. 1B) (Callot et al., 2007; Jahani et al., 2009) and the linkage of different folds (N of Firuzabad; Fig. 2) (Ramsey et al., 2008). Detachment folding in the cover was accompanied by the development of the S-propagating and NNW-oriented right-lateral Kareh Bas Fault (Fig. 14C). Jahani et al. (2017) propose that the dextral strike-slip faults in the western Fars Arc decorated with salt extrusions represent tear faults controlled by two factors: (1) greater advance of the cover above thicker Hormuz salt in the drowthrown side of old down-to-the-E basement normal faults (i.e., lower basal friction); and (2) presence of

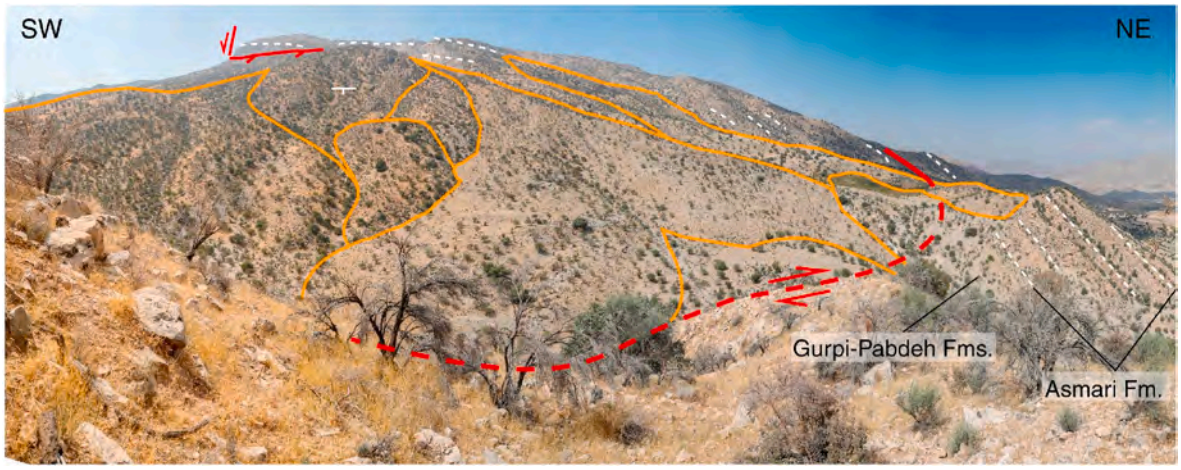

Fig. 13. Cluster of rock slide-flows developed on dip slopes on the NE limb of the Dandejan W Anticline. The development of these landslides has been favoured by normal faults in the upper part of the slopes, the presence of weak Kazhdumi marls and shales underlying the Sarvak limestone and fluvial incision at the foot of the slope guided by the Kareh Bas Fault.

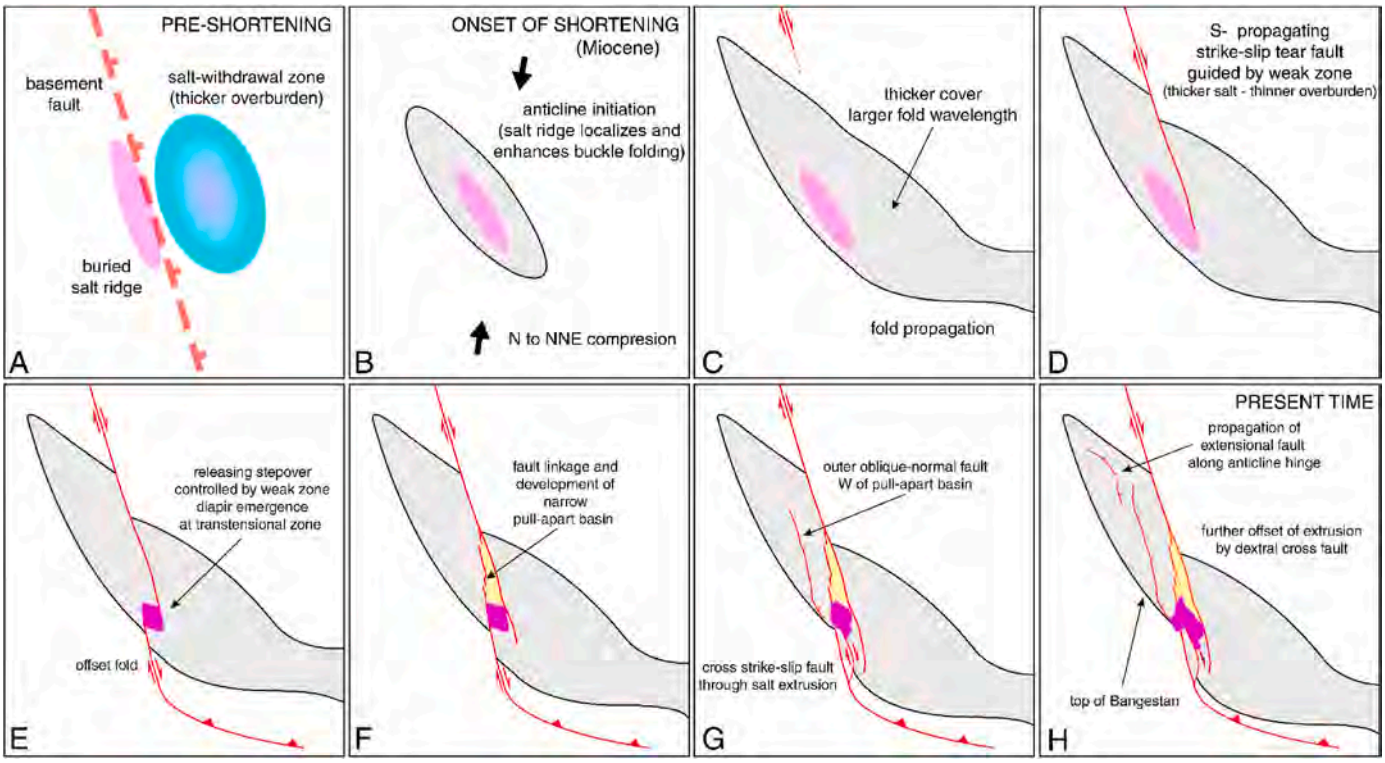

Fig. 14. Evolutionary model for the Kareh Bas-Dandenjan fault-diapir system. See explanation in the text.

weak zones related to rows of precursor diapirs (Fig. 14C and D). According to this concept, the Kareh Bas Fault is a supra-salt fault whose trace is guided by mechanical weaknesses conditioned by an old infra-salt basement fault. The onset of strike-slip faulting at Dandenjan most probably postdates the initiation of folding in the Miocene. Assuming that the horizontal slip rate of 3.1–3.7 mm/yr obtained by GPS measurements for the Kareh Bas Fault (Tavakoli et al., 2008) has been constant, and considering the cumulative offset of 4.4–5.7 km measured in this work at Dandenjan Anticline, it can be estimated that the onset of activity at this site occurred at around 1.8–1.2 Ma. This age is considerably younger than the onset of vigorous folding recorded by the base of the Bakhtyari Formation and situated by magneto-chronological studies at about 3.8 Ma on folds at a slightly more southern trend (Kuh-e-Ghol Anticline, labelled in Fig. 1B; Ruh et al., 2014). This time lag, although rather speculative, supports that the onset of strike-slip faulting at the site is younger than folding, as suggested by other authors (e.g., Authemayou et al., 2006).

The presence of a precursor salt diapir likely induced the segmentation of the S-propagating right-lateral Kareh Bas Fault and the formation of the narrow right releasing stepover mapped in this work (Figs. 5 and 14E). Mann (2007) illustrates that crustal heterogeneities promote the development of stepovers. Analogue experiments of strike-slip fault development reveal that weak zones (e.g., diapirs, magma bodies, pre-existing structures) can function as barriers for rupture propagation favouring fault segmentation and the development of stepovers (Holohan et al., 2008; Dooley and Schreurs, 2012). Experiments show that propagating Riedel shears tend to deflect and increase their angle with respect to the principal shear direction as they approach the weak zone, resulting in the development of a stepover centred at the weak zone (Dooley and Schreurs, 2012). Extension at the releasing stepover thinned and weakened the overburden eventually led to the extrusion of the Dandejan Diapir fed by salt squeezed from the adjacent anticline.

In previous works, various interpretations have been proposed on the mechanical relationships between the dextral strike-slip faults of the western Fars Arc and the associated salt extrusions. (1) Gaps created by rotation of basement blocks: Hessami et al. (2001b) propose that the diapirs rise through gaps in the sedimentary cover formed by rotation of fault-bounded basement blocks about vertical axes, aiding extension along the Zagros Belt. (2) Neoformation of salt diapirs related to the interaction of strike-slip and shortening structures: Koyi et al. (2008), based on analogue models, indicate that diapirs intrude through pull-apart basins and damage zones formed by the interaction between basement strike-slip faults and folds and thrusts with oblique slip. They ruled out the alternative of the reactivation of precursor diapirs with a thin overburden assuming that the diapirs were initiated during the late Cenozoic collision. (3) Releasing stepovers: Talbot and Alavi (1996) contend that diapirs rise into rhombic openings pulled apart at releasing stepovers between en echelon parallel faults. They suggest that before the Cenozoic shortening the diapirs were dominantly N-trending structures, like the salt structures south of the Zagros deformation front. (4) Extrusion of squeezed salt through tear faults: Jahani et al. (2017) sustain that precursor diapirs controlled the development of tear faults and that the diapirs, rejuveneated by folding, emerged through the strike-slip faults. These authors, based on the existing geological maps, suggest a lack of relationship between pull-apart zones and salt extrusions, with the exception of Salamati, located on a releasing bend (Fig. 2). Our mapping supports that transtension associated with a narrow releasing stepover (Talbot and Alavi, 1996), together with the squeezing of salt from the core of Dandenjan anticline (i.e., contractional loading; Jahani et al., 2017), induced the emergence of a precursor diapir (options 3 and 4 above). Talbot and Aftabi (2004) also documented salt extrusions associated with releasing stepovers in the Qom Basin, central Plateau of Iran. The lack of relationship with a pull-apart zone suggested by other authors seems to be related to the small scale of the previous geological maps (e.g., Perry et al., 1965).

The northern propagation of the southern fault strand through the development of a right-stepping fault array eventually led to fault linkage and the development of the narrow triangle-shaped Dandenjan pull-apart basin, characterised by a high elongation ratio (length/width:

6.1) (Fig. 14F). Analogue experiments indicate that the geometry of pull-apart basins associated transtensional stepovers are controlled by two main factors (Mann et al., 1983; Richard et al., 1995; Sims et al., 1999; Smit et al., 2008a, 2008b; Dooley and Schreurs, 2012): (1) separation of fault segments; the shorter the separation, the narrower the basin; (2) degree of overlapping versus underlapping of the faults; basins at overlapping stepovers attain a rhomboidal or box geometry, whereas those at underlapping stepovers are commonly spindle-shaped. Experimental models also suggest that with a thick ductile layer (i.e., less coupling between basement and overburden), the angle between the basin axis and the principal deformation zone decreases (Sims et al., 1999; Le Calvez and Vendeville, 2002; Smit et al., 2008a, 2008b; Dooley and Schreurs, 2012), which aligns with the case of the Dandenjan pull-apart basin (Fig. 5). Experiments of pull-apart basin development show that at advanced stages cross-basin faults tend to form linking the stepped principal displacement zone (Dooley et al., 2004, 2007; Wu et al., 2009; Dooley and Schreurs, 2012). The fault within the stepover, that dextrally offsets the Dandenjan salt extrusion some 2.4 km, seems to represent this type of late-stage fault (Figs. 11 and 14G).

The E-dipping normal fault array developed across the Dandenjan W Anticline and mostly parallel to the pull-apart basin seems to be related to the westward propagation of transtensional deformation. These are most probably oblique normal faults with dextral displacement component, but unfortunately no outcrops were found to measure kinematic indicators. This left-stepping normal fault system likely propagated to the north, as supports the decreasing throw in that direction. The deviation of the fault strike to a NW fold-parallel orientation is probably related to the adaptation of the rupture to a weak zone associated with the salt-cored anticline (Fig. 14H). The geomorphic features associated with the faults bounding the Dandenjan pull-apart basin and the western fault reveal their recency and most probably current activity (linear fronts with triangular facets, well-expressed enclosed grabens, disrupted drainage). The widespread ongoing extension that occurs north of the Dandenjan Diapir is likely related to local transtension induced by thickness variations in the salt detachment and faster translation of the cover above thicker salt. This could be achieved by an oblique antithetically skewed boundary step in the Hormuz salt; for instance, a right stepping stepover or bend in the down-to-the-east basement fault (see Fig. 12.32 in Jackson and Hudec, 2017).

The concept of the southward propagation of the Kareh Bas strike-slip fault and the successive emergence of salt diapirs rejuvenated by contractional loading at growing anticlines is supported by the topography and morphometry of the salt extrusions. They show a N-to-S morphological gradation from a highly degraded dome (Salamati) to an expanding salt fountain with a well-defined summit dome and radiating namakiers (Jahani) (Fig. 4). Moreover, the clear spatial association between the salt extrusions and the strike-slip fault indicates that the surface rupture provides the path for salt emergence. Salamati (Jackson and Hudec, 2017; Jahani et al., 2017) and Dandenjan occur at transtensional zones, whereas full understanding of the structural setting of the other extrusion require additional mapping. Barnhart and Lohman (2012), in a regional InSAR study of salt extrusions in the Fars Arc (Envisat C-band data, 2003–2010; detection threshold ca. 3 mm/yr), identify as continuously active the three diapirs associated with the southern segments of the Kareh Bas fault zone (Konarsiah, Jahani and Bahar), but not the remaining ones to the north (Dandenjan, Meygor and Salamati; Fig. 2). The salt extrusions in the eastern Fars Arc, mostly lacking any relationship with surface faults, do not show a clear age gradation consistent with the southward propagation of the collisional shortening (Talbot and Alavi, 1996; Jahani et al., 2007). This suggests that the evolution of the salt extrusions in that region is controlled by a more complex set of factors, such as: (1) the timing of salt breakout (e.g., Gutiérrez et al., 2023b); (2) the variable size and geometry of the precursor salt diapirs (e.g., stock, wall) and the size of the opening through which it extrudes; (3) the rate of contractional loading; (4) development of primary and secondary welds; (5) climate and erosion, dominated by dissolution (i.e., aridity increase towards the coast; Bruthans et al., 2008).

6.2. Seismic hazards associated with the Kareh Bas fault

Three main earthquake-related hazards are associated with the Kareh Bas Fault, with a significant slip rate (3.4 ± 0.3 mm/yr) comparable with that of the Kazerun Fault (Tavakoli et al., 2008): (1) coseismic surface rupture; (2) strong motion; and (3) earthquake-induced landslides. Field evidence indicates that the Kareh Bas Fault has experienced multiple meter-scale surface ruptures in late Quaternary times (Fig. 3; Supplementary material Fig. SP1, SP2). The minimum sequence of two surface-deforming events inferred from the analysed outcrop of the fault on a +40 m terrace of the Dalaki River suggests recent $M_w \geq 6.5$ earthquakes sourced for the Kareh Bas S fault segment. According to Youngs et al. (2003), based on data from different types of faults, the probability of having a primary surface rupture associated with M_w 6, 6.5, 7 and 7.5 earthquakes are around 45%, 70%, 87% and 95%, respectively. More updated regressions generated by Pizza et al. (2023) from 139 strike-slip earthquake events indicate probabilities of around 15%, 55%, 95% and 100%, which are considerably lower than those of Youngs et al. (2003) for M_w 6 and 6.5. The set of dates obtained by ^{10}Be cosmogenic exposure age for terraces of the Mand and Dalaki rivers south of the Kareh Bas Fault by Oveisi et al. (2009) suggest that the paleoearthquakes identified in the +40 m terrace of the Dalaki River occurred in the late Pleistocene.

Key elements in the characterisation of fault sources for seismic hazard analysis are the expected earthquake magnitude and recurrence (e.g., Wesnousky, 1986; McCalpin, 2009). Earthquake magnitude largely depends on the size of the fault sources (length, rupture area) and the role played by fault segmentation in the propagation of ruptures. The Kareh Bas fault system, with an aggregate length of 220 km, comprises three geometric segments, likely controlled by weak zones associated with precursor salt diapirs underlain by basement faults (Jahani et al., 2017). The 120 km long Kareh Bas N segment and the 56 km long Kareh Bas S segments are separated by a 14 km long thrust bend (Dandenjan reverse fault). The right step between the overlapping Kareh Bas S segment and the 44 km long Kareh Bas SW segment is around 12 km wide. The large size of these discontinuities indicate that the different cartographic segments most probably behave as independent seismogenic sources. Biasi and Wesnousky (2016), based on 46 mapped strike-slip surface ruptures infer that geometric discontinuities in fault traces larger than 6 km are expected to stop ruptures in all cases, acting as barriers for seismogenic segments. Biasi and Wesnousky (2017) also indicate that bends in strike-slip faults at high angles like the Dandenjan Thrust (ca. 60°) are expected to stop ruptures. According to the scaling relationship between earthquake magnitude and surface rupture length for strike-slip faults (43 historical events, correlation coefficient 0.91) of Wells and Coppersmith (1994), the N, S and SW segments of the Kareh Bas Fault might generate earthquakes with moment magnitudes M_w = 7.5, 7.1 and 7.0, respectively, assuming that they rupture along their entire length. Slightly lower values are obtained with the more recent orthogonal regressions produced by Thingbaijam et al. (2017) using rupture models (fault rupture length) of well-instrumented earthquakes (M_w = 7.4, 6.9 and 6.7, respectively).

A controversial issue with implications for seismic hazard assessment is whether the dextral strike-slip faults of the western Fars Arc are confined to the supra-salt cover or penetrate into the basement, which has impact on the potential rupture area and thus earthquake magnitude. Berberian (1995) sustains that they are basement faults that have caused significant right-lateral offset on inferred longitudinal blind reverse faults, such as the Mountain Front Fault. Talbot and Alavi (1996), Hessami et al. (2001b) and Sepehr and Cosgrove (2005) contend that these are faults rooted in the Arabian basement that controlled sedimentation before the Zagros orogeny, during which they experienced reactivation as wrench faults. Authemayou et al. (2006) consider

that these faults, splayed from the Main Recent Fault, affect both the basement and the cover. Tavakoli et al. (2008) suggest that displacement on the Kazerun Fault system should involve the basement, since in case it would be a tear fault related to differential basal friction, the greatest slip should occur along the Borazjan segment, closer to the deformation front. In contrast, Jahani et al. (2017) suggest that the displacement along these strike-slip faults is restricted to the sedimentary cover, around 12–15 km thick, and that it is unlikely that the basement faults are reactivated as strike-slip faults under the current stress regime. The interpretation whereby the strike-slip faults are confined to the cover and related to mechanical heterogeneities imposed by the Hormuz salt (i.e., thickness variations, rows of precursor diapirs) is supported by two lines of evidence: (1) the foci of most of the strike-slip faults in the western Fars Arc are situated above the salt detachment, with some exceptions in the Karezun fault segment (Karasözen et al., 2019, Fig. 1B); and (2) the southern termination of the faults roughly coincides with the boundary of the region where salt diapirs are lacking, corresponding to the Qatar-Fars Arc, an intrabasinal high where thinner Hormuz salt was deposited (Jahani et al., 2017) (Fig. 1B). This supports the concept of strike-slip earthquakes mostly nucleated in the supra-salt "competent group", rather than in the "rigid basement" (Nissen et al., 2011). Nonetheless, this alternative does not have a significant impact on the potential earthquake magnitude, given the high depth of the salt detachment (lower mobile group). The expected moment magnitudes for the N, S and SW segments based on the regression for rupture area (83 strike-slip events, 0.96 correlation coefficient) considering a seismogenic depth of 12 km and a vertical attitude for the fault are M_w = 7.2, 6.9 and 6.8, respectively (Wells and Coppersmith, 1994), which are comparable with those derived from fault length. More recent orthogonal regressions produced by Thingbaijam et al. (2017) using rupture models (rupture area) of well-instrumented earthquakes provide slightly lower magnitudes (M_w = 7.1, 6.7 and 6.6, respectively). The concept whereby large earthquakes ($M_w \geq 6.5$) do not necessarily require basement faults has implications for interpreting the source of the 1972, M_s 6.9 reverse fault earthquake, located at the eastern prolongation of the Surmeh reverse fault (Figs. 1B and 2). This event, which killed more than 5010 people, is widely regarded as a paradigmatic example of an earthquake generated by a blind basement reverse fault in the Zagros. However, this notion is not in agreement with its focal depth of 10 km (error <3 km; Karasözen et al., 2019) (Table 1; Dewey and Grantz, 1973; Berberian, 1995, 2014; Karasözen et al., 2019), situated above the Hormuz salt according to recent data on the depth of the Hormuz salt based on seismic lines (Jahani et al., 2009, 2017). The relevant implication for seismic hazard assessment is that large damaging earthquakes of magnitude M = 6.5–7 could also be generated by ruptures above the deep salt detachment.

Large bedrock landslides show a striking frequency increase in the vicinity of the Kareh Bas fault system (Figs. 2 and 5). The mapped slope movements include very large landslides up to 25 km^2 and catastrophic long runout (up to 7 km) rock avalanches with an extremely high damaging capability (Fig. 12). Almost 90% of the 26 mapped landslides occur at a distance of ≤10 km. This spatial pattern can be attributed to the combined effect of two factors of triggering and preparatory nature (Glade and Crozier, 2005): (1) Strong ground motion related to large earthquakes sourced at the Kareh Bas fault triggers slope failures (coseismic landslides) in the vicinity of the fault, resulting is spatial clusters of landslides (Strom, 2015). Rodriguez et al. (1999), based on a large database of coseismic landslides, show that earthquakes within the magnitude range 6.5–7 can trigger landslides at a maximum distance of around 100 km, and that most of the slope movements occur at less than 20 km from the fault trace. (2) The active strike-slip Kareh Bas Fault creates favourable conditions for landslide development through various processes, including the creation of fault-parallel escarpments by the lateral offset of anticlinal ridges (Figs. 2 and 10); the weakening of the rock mass by the master fault and associated structures (Fig. 13); and the weakened fault zone can guide the path of drainage that enhance local relief by fluvial incision (Fig. 13). The documented fault-landslide spatial association has potential practical implications. On the one hand, active seismogenic faults can be highly useful to assess landslide susceptibility (i.e., spatial prediction). On the other hand, comprehensive cartographic landslide inventories may reveal spatial clusters potentially attributable to both surface and blind seismogenic faults. Additionally, proper landslide identification has important implications for geological mapping, because shallow gravitational deformations related to slope movements (Fig. SP6) can be erroneously interpreted as tectonic structures related to regional stress fields. This is illustrated by extensive putative fault breccias (ca. 25 km^2) mapped in the vicinity of Salamati Diapir (GSI, 1996a), which correspond to landslides 7 and 8 in Fig. 2.

7. Conclusions

The local progressive unconformity in the Gachsaran Formation associated with the Dandenjan diapir and anticline records the inception of folding in the Miocene. The presence of a precursor diapir likely advanced, localized and enhanced folding. An evolutionary model, largely based on cartographic and field data, is proposed for the KarehBas and Dandenjan strike-slip fault and diapir system. The precursor Dandenjan Diapir controlled the segmentation of the south-propagating Kareh Bas fault resulting in the development of a narrow releasing stepover. Transtension associated with the stepover favoured the extrusion of the diapir, fed by salt squeezed from the adjacent anticline, and resulted in the development of the Dandenjan pull-apart basin. Extension has propagated to the west of the pull-apart basin as revealed by oblique normal faults with conspicuous geomorphic expression superimposed across the Dandenjan Anticline. This widespread extension likely accommodates transtension induced by differential translation of the supra-salt cover above Hormuz salt with spatially variable thickness controlled by a basement fault (e.g., basement fault locally skewed antithetically to the overall slip direction).

Morphological and morphometric data (local relief, volume, average thickness) indicate that the salt extrusions associated with the Kareh Bas fault system display a N-S gradation in their evolutionary stage, supporting a chronological sequence with the emergence of progressively younger extrusions towards the south, as the Kareh Bas propagated towards the foreland. This row of diapirs offers the opportunity to investigate the geomorphic evolution of salt extrusions applying the ergodic concept, substituting time by space.

Exposures showing evidence of Quaternary deformation associated with the Kareh Bas fault have been documented for the first time, including recurrent meter-scale coseismic surface deformation recorded by late Pleistocene terrace deposits of the Dalaki River.

The Kareh Bas fault system has the capability to generate large M_w 6.5–7 earthquakes despite its segmentation and even if ruptures are restricted to the supra-salt cover, given the high depth of the salt detachment (12–15 km). A similar concept could be applied to the 1972, M_s 6.9 Qir (or Ghir) earthquake (focal depth 10 km), widely regarded as one of the two largest earthquakes generated by blind reverse faults in the seismic history of the Zagros.

The much higher spatial frequency and clustering of large landslides in the vicinity of the Kareh Bas fault system (<10 km) suggests that strong ground motion related to large earthquakes sourced from that fault together with local conditions created by the structure play a major causal role. This clear spatial association has practical implications for landslide susceptibility assessment and the identification of seismogenic sources in the Zagros. Detailed mapping reveals that the deposits of some large landslides have been erroneously identified in geological maps as extensive fault breccias associated with the Kareh Bas Fault.

CRediT authorship contribution statement

Francisco Gutiérrez: Writing – original draft, Software, Resources, Project administration, Methodology, Investigation, Funding

acquisition, Formal analysis, Data curation, Conceptualization. **Issa Ilyati:** Data curation. **Mohsen Rezaei:** Writing – review & editing, Project administration. **Mehdi Zarei:** Writing – review & editing, Project administration. **Michael Hudec:** Writing – review & editing, Conceptualization.

Declaration of competing interest

The authors declare the following financial interests/personal relationships which may be considered as potential competing interests:

Francisco Gutierrez reports financial support was provided by Ministerio de Ciencia e Innovación, Spain. If there are other authors, they declare that they have no known competing financial interests or personal relationships that could have appeared to influence the work reported in this paper.

Data availability

Data will be made available on request.

Acknowledgements

The authors are very grateful to the Major of Dandenjan village (Mr. Ardeshir Kamali) for logistical support. Edwin Nissen and Ezgi Karasözen kindly provided data from their relocated earthquake catalogue of the Fars Arc. Insightful comments from Álvaro González and Eduard Roca helped with the interpretation of the cartographic and field data. The detailed work conducted by tow anonymous reviewers significantly contributed to improve the quality of the article. The work has been supported by the Salvador de Madariaga grant (PRX22/00029) and project DIAPERNO (PID 2021-123189NB-I00) of the Spanish Government (Ministerio de Ciencia e Innovación). The TanDEM-X digital elevation models were provided by theGerman Aerospace Center (grant DEMGEOL288).

Appendix A. Supplementary data

Supplementary data to this article can be found online at https://doi.org/10.1016/j.jsg.2024.105239.

References

Abirifard, M., Raeisi, E., Zarei, M., Zare, M., Filippi, M., Bruthans, J., Talbot, C.J., 2017. Jahani Salt Diapir, Iran: hydrogeology, karst features and effect on surrounding environment. Int. J. Speleol. 46, 445–457.
Adineh, S., Závada, P., Bruthans, J., Cofrade, G., Zare, M., 2023. Growth of a salt diapir in an anticline. A record from the Cenozoic halokinetic sequences in the Zagros fold and thrust belt, Iran. J. Struct. Geol. 178, 105004.
Ambraseys, N.N., Melville, C.P., 1982. A History of Iranian Earthquakes. Cambridge University Press, Cambridge, p. 219.
Ambraseys, N.N., Jackson, J.A., 1998. Faulting associated with historical and recent earthquakes in the eastern Mediterranean region. Geophys. J. Int. 133, 390–406.
Authemayou, C., Chardon, D., Bellier, O., Malekzadeh, Z., Shabanien, E., Abbassi, M., 2006. Late Cenozoic partitioning of the oblique plate convergence in the Zagros fold-and-thrust belt (Iran). Tectonics 25, TC3002.
Authemayou, C., Bellier, O., Chardon, D., Benedetti, L., Malekzade, Z., Claude, C., Angeletti, B., Shabanian, E., Abbassi, M.R., 2009. Quaternary slip-rates of the Kazerun and the Main Recent Faults: active strike-slip partitioning in the Zagros fold-and-thrust belt. Geophys. J. Int. 178, 524–540.
Bachmanov, D.M., Trifonov, V.G., Hessami, K.T., Kozhurin, A.I., Ivanova, T.P., Rogozhin, E.A., Hademi, M.C., Jamali, F.H., 2004. Active faults in the Zagros and Central Iran. Tectonophysics 380, 221–241.
Bahroudi, A., Koyi, H.A., 2004. Tectono-sedimentary framework of the Gachsaran Formation in the Zagros foreland basin. Mar. Petrol. Geol. 21, 1295–1310.
Baker, C., Jackson, J., Priestley, K., 1993. Earthquakes on the kazerunline in the Zagros mountains of Iran: strike-slip faulting within a fold-and-thrust belt. Geophysics Journal International 115, 41–61.
Barnhart, W.D., Lohman, R.B., 2012. Regional trends in active diapirism revealed by mountain range-scale InSAR time series. Geophys. Res. Lett. 39, L08309.
Barnhart, W.D., Lohman, R.B., Mellors, R.J., 2013. Active accommodation of plate convergence in Southern Iran: earthquake locations, triggered aseismic slip, and regional strain rates. J. Geophys. Res. Solid Earth 118, 5699–5711.
Berberian, M., 1981. Active faulting and tectonics of Iran. In: Gupta, H.K., Delany, F.M. (Eds.), Zagros-Hindu Kush-Himalaya Geodynamic Evolution. American Geophysical Union, Geodynamic Series, vol. 3, pp. 33–69.
Berberian, M., 1995. Master "blind" thrust faults hidden under the Zagros folds: active basement tectonics and surface morphotectonics. Tectonophysics 241, 193–224.
Berberian, M., 2014. Earthquakes and Coseismic Surface Faulting on the Iranian Plateau. Elsevier, Amsterdam, p. 776.
Berberian, M., Tchalenko, J.S., 1976. Earthquakes of Southern Zagros (Iran): Bushehr Region, vol. 39. Geological Survey of Iran, pp. 343–369.
Berberian, M., Papastamatiou, D., 1978. Khurgu (North Bandar Abbas, Iran) earthquake of March 21, 1977: a preliminary field report and seismotectonic discussion. Bull. Seismol. Soc. Am. 68, 411–428.
Biasi, G.P., Wesnousky, S.G., 2016. Steps and gaps in ground ruptures: empirical bounds on rupture propagation. Bull. Seismol. Soc. Am. 106, 1110–1124.
Biasi, G.P., Wesnousky, S.G., 2017. Bends and ends of surface ruptures. Bull. Seismol. Soc. Am. 107, 2543–2560.
Bordenave, M.L., Hegre, J.A., 2010. Current distribution of oil and gas fields in the Zagros Fold Belt of Iran and contiguous offshore as the result of the petroleum systems. In: Leturmy, P., Robin, C. (Eds.), Tectonic and Stratigraphic Evolution of the Zagros and Makran during the Mesozoic-Cenozoic, vol. 330. Geological Society, London, Special Publication, pp. 291–353.
Brettis, B., Bartl, N., Grasemann, B., 2011. Lateral fold growth and linkage in the Zagros fold and thrust belt (Kurdistan, NE Iraq). Basin Res. 223, 615–630.
Bruthans, J., Asadi, N., Filippi, M., Vihelm, Z., Zare, M., 2008. A study of erosion rates on salt diapir surfaces in the Zagros Mountains, SE Iran. Environ. Geol. 53, 1079–1089.
Burberry, C.M., Cosgrove, J.W., Liu, J.G., 2008. Spatial arrangement of fold types in the Zagros Simply Folded Belt, Iran, indicated by landform morphology and drainage pattern characteristics. J. Maps 4, 417–430.
Burberry, C.M., Cosgrove, J.W., Liu, J.G., 2010. A Study of Fold Characteristics and Deformation Style Using the Evolution of the Land Surface: Zagros Simply Folded Belt, vol. 330. Geological Society, London, Special Publications, Iran, pp. 139–154.
Callot, J.P., Jahani, S., Letouzey, J., 2007. The role of pre-existing diapirs in fold and thrust belt development. In: Lacombe, O., Roure, F., Lavé, J., Vergés, J. (Eds.), Thrust Belts and Foreland Basins. Springer, Berlin, pp. 1–17.
Collignon, M., Yamato, P., Castelltort, S., Kaus, B.J., 2016. Modeling of wind gap formation and development of sedimentary basins during fold growth: application to the Zagros Fold Belt, Iran. Earth Surf. Process. Landforms 41, 1521–1535.
Cotton, J.T., Koyi, H.A., 2000. Modeling of thrust fronts above ductile and frictional detachments. Application to structures in the Salt Range and Potwar Plateau, Pakistan. Geol. Soc. Am. Bull. 112, 351–363.
Cunningham, W.D., Mann, P., 2007. Tectonics of strike-slip restraining and releasing bends. In: Cunningham, W.D., Mann, P. (Eds.), Tectonics of Strike-Slip Restraining and Releasing Bends, vol. 290. Geological Society, London, Special Publications, pp. 1–12.
De Waele, J., Gutiérrez, F., 2022. Karst Hydrogeology, Geomorphology and Caves. Wiley, Chichester.
Dewey, J.W., Grantz, A., 1973. The Ghir earthquake of April 10, 1972 in the Zagros Mountains of southern Iran: seismotectonic aspects and some results of a field reconnaissance. Bull. Seismol. Soc. Am. 63, 2071–2090.
Dooley, T., Monastero, F., Hall, B., McClay, K.R., Whitehouse, P., 2004. Scaled sandbox modelling of transtensional pull-apart basins: applications to the Coso geothermal system. Trans. Geoth. Resour. Counc. 28, 637–641.
Dooley, T., Monastero, F.C., McClay, K.R., 2007. Effects of a weak crustal layer in a transtensional pull-apart basin: results from a scaled physical modeling study. Eos 88 (Abstract V53F–04).
Dooley, T.P., Schreurs, G., 2012. Analogue modelling of intraplate strike-slip tectonics: a review and new experimental results. Tectonophysics 574–575, 1–71.
Edgell, H.S., 1996. Salt tectonism in the Persian Gulf basin. In: Aslop, G.I., Blundell, D.J., Davison, I. (Eds.), Salt Tectonics, vol. 100. Geological Society London Special Publication, pp. 129–151.
Ezzati Asl, M., Faghih, A., Mukherjee, S., Soleimany, B., 2019. Style and timing of salt movement in the Persian Gulf basin, offshore Iran: insights from halokinetic sequences adjacent to the Tonb-e-Bozorg salt diapir. J. Struct. Geol. 122, 116–132.
Faghih, A., Nezamzadeh, I., Kusky, T., 2016. Geomorphometric evidence of an active pop-up structure along the sabzpushan fault zone, Zagros mountains, SW Iran. J. Earth Sci. 27, 945–954.
Faghih, A., Ezati-Asl, M., Mukherjee, S., Soleimany, B., 2019. Characterizing halokinesis and timing of salt movement in the Abu Musa salt diapir, Persian Gulf, offshore Iran. Mar. Petrol. Geol. 105, 338–352.
Fakhari, M.D., Axen, G.J., Horton, B.K., Hassanzadeh, J., Amini, A., 2008. Revised age of proximal deposits in the Zagros foreland basin and implications for Cenozoic evolution of the High Zagros. Tectonophysics 451, 170–185.
Ghanadian, M., Faghih, A., Abdolahi Fard, I., Kusky, T., Maleki, M., 2017a. On the role of incompetent strata in the structural evolution of the Zagros Fold-Thrust Belt, Dezful Embayment, Iran. Mar. Petrol. Geol. 81, 320–333.
Ghanadian, M., Faghih, A., Grasemann, B., Abdolahi Fard, I., Maleki, M., 2017b. Analogue modeling of the role of multi-level decollement layers on the geometry of orogenic wedge: an application to the Zagros Fold–Thrust Belt, SW Iran. Int. J. Earth Sci. 106, 2837–2853.
Ghazipour, N., Simpson, G., 2017. Size distribution and controls of landslides in the Zagros mountain belt (Iran). Tectonic evolution, collision, and seismicity of Southwest Asia. In: Sorkhabi, E. (Ed.), Tectonic Evolution, Collision and Seismicity of Southwest Asia. In Honor of Manuel Berberian's Forty-Five Years of Research Contributions, vol. 525. The Geological Society of America Special Paper, pp. 1–21.

Glade, T., Crozier, M., 2005. The nature of landslide hazard impact. In: Glade, T., Anderson, M., Crozier, M. (Eds.), Landslide Hazard and Risk. Wiley, Chichester, pp. 43–74.
GSI, 1996a. Geological Map of Iran 1:100.000 Series. Darenjan Sheet. Geological Survey of Iran, Tehran.
GSI, 1996b. Geological Map of Iran 1:100.000 Series. Farrashband Sheet. Geological Survey of Iran, Tehran.
Gutiérrez, F., Lizaga, I., 2016. Sinkholes, collapse structures and large landslides in an active salt dome submerged by a reservoir. The unique case of the Ambal ridge in the Karun River, Zagros Mountains, Iran. Geomorphology 254, 88–103.
Gutiérrez, F., Deirnik, H., Zarei, M., Medialdea, A., 2023a. Geology, geomorphology and geochronology of the coseismic? Emad Deh rock avalanche associated with a growing anticline and a rising salt diapir, Zagros Mountains, Iran. Geomorphology 421, 108527.
Gutiérrez, F., Zarei, M., Hudec, M.R., Deirnik, H., 2023b. Normal faulting and landsliding in morpho-structural domes related to buried salt stocks, Zagros Mountains, Iran. Insights into salt breakout. Mar. Petrol. Geol. 155, 106376.
Harrison, J.V., 1930. The geology of some salt-plugs in Laristan, southern Persia. Quarterly Journal of the Geological Society 86, 463–522.
Hassanpour, J., Jahani, S., Ghassemi, M.R., Alavi, S.A., Zeinali, F., 2018. Evolution of the Karebas Fault System and adjancent folds, central Zagros fold-and-thrust belt, Iran: role of pre-existing halokinesis (salt structures and minibasins) and detachment levels. J. Asian Earth Sci. 164, 125–142.
Hessami, K., Koyi, H.A., Talbot, C.J., Tabasi, H., Shabanian, E., 2001a. Progressive unconformities within an evolving foreland fold–thrust belt, Zagros Mountains. J. Geol. Soc. 158, 969–981.
Hessami, K., Koyi, H.A., Talbot, C.J., 2001b. The significance of strike-slip faulting in the basement of the Zagros fold and thrust belt. J. Petrol. Geol. 24, 5–28.
Holohan, E.P., van Wyk de Vries, B., Troll, V.R., 2008. Analogue models of caldera collapse in strike-slip tectonic regimes. Bull. Volcanol. 70, 773–796.
Homke, S., Vergés, J., Garcés, M., Emami, H., Karpuz, R., 2004. Magnetostratigraphy of miocene-pliocene Zagros foreland deposits in the front of the push-e kush arc (lurestan province, Iran). Earth Planet Sci. Lett. 225, 397–410.
Jackson, J.A., 1980. Reactivation of basement faults and crustal shortening in orogenic belts. Nature 283, 343–346.
Jackson, M.P.A., Hudec, M.R., 2017. Salt Tectonics. Principles and Practice. Cambridge University Press, Cambridge, p. 510.
Jahani, S., Callot, J.P., Frizon de Lamotte, D., Letouzey, J., Leturmy, P., 2007. The salt diapirs of the eastern Fars Province (Zagros, Iran): a brief outline of their past and present. In: Lacombe, O., Roure, F., Lavé, J., Vegés, J. (Eds.), Thrust Belts and Foreland Basins. Springer, Berlin, pp. 289–308.
Jahani, S., Callot, J.P., Letouzey, J., Frizon de Lamotte, D., 2009. The eastern termination of the Zagros Fold-and-Thrust Belt, Iran: structures, evolution, and relationships between salt plugs, folding, and faulting. Tectonics 28, TC6004.
Jahani, S., Hassanpour, J., Mohammadi-Firouz, S., Letouzey, J., de Lamotte, D.F., Alavi, S.A., Soleimany, B., 2017. Salt tectonics and tear faulting in the central part of the Zagros Fold-Thrust Belt, Iran. Mar. Petrol. Geol. 86, 426–446.
Karasözen, E., Nissen, E., Bergman, E.A., Ghods, A., 2019. Seismotectonics of the Zagros (Iran) from orogen-wide, calibrated earthquake relocations. J. Geophys. Res. Solid Earth 124, 9109–9129.
Khadivi, S., Mouthereau, F., Larrasoaña, J.C., Vergés, J., Lacombe, O., Khademi, E., Beamud, E., Melinte-Dobrinescu, M., Suc, J.P., 2010. Magnetochronology of synorogenic Miocene foreland sediments in the Fars Arc of the Zagros folded belt (SW Iran). Basin Res. 22, 918–932.
Kent, P.E., 1979. The emergent Hormuz salt plugs of southern Iran. J. Petrol. Geol. 2, 117–144.
Koyi, H.A., Ghasemi, A., Hessami, K., Dietl, C., 2008. The mechanical relationship between strike-slip faults and salt diapirs in the Zagros fold–thrust belt. J. Geol. Soc. 165, 1031–1044.
Le Calvez, J.H., Vendeville, B.C., 2002. Experimental designs to model along strike-slip fault interaction. In: Schellart, W.P., Passchier, C. (Eds.), Analogue Modeling of Large-Scale Tectonic ProcessesJournal of the Virtual Explorer, vol. 7, pp. 7–23.
Letouzey, J., Sherkati, S., 2004. Salt movement, tectonic events, and structural style in the central Zagros Fold and thrust belt (Iran). In: 24th Annual GCSSEPM Foundation. Bob F. Perkins Research Conference: Salt-Sediment Interactions and Hydrocarbon Prospectivity: Concepts, Applications, and Case Studies for the 21st Century, Gulf Coast Section. Society for Sedimentary Geology, Houston, Texas.
Leturmy, P., Molinaro, M., de Lamotte, D.F., 2010. Structure, timing and morphological signature of hidden reverse basement faults in the Fars Arc of the Zagros (Iran). In: Leturmy, P., Robin, C. (Eds.), Tectonic and Stratigraphic Evolution of Zagros and Makran during the Mesozoic-Cenozoic, vol. 330. Geological Society, London, Special Publications, pp. 121–138.
Lohman, R.B., Simons, M., 2005. Locations of selected small earthquakes in the Zagros mountains. G-cubed 6, Q03001.
Macedo, J., Marshak, S., 1999. Controls on the geometry of fold-thrust belt salients. Geol. Soc. Am. Bull. 111, 1808–1822.
Maggi, A., Jackson, J.A., Priestley, K., Baker, C., 2000. A re-assessment of focal depth distribution in southern Iran, the Tien Shan and northern India; do earthquakes really occur in the continental mantle? Geophys. J. Int. 143, 629–661.
Mann, P., 2007. Global catalogue, classification and tectonic origins of restraining and releasing bends on active and ancient strike-slip fault systems. In: Cunningham, W. D., Mann, P. (Eds.), Tectonics of Strike-Slip Restraining and Releasing Bends, vol. 290. Geological Society, London, Special Publications, pp. 13–142.
Mann, P., Hempton, M.R., Bradley, D.C., Burke, K., 1983. Development of pull-apart basins. J. Geol. 91, 529–554.
McCalpin, J.P., 2009. Application of paleoseismic data to seismic hazard assessment and neotectonic research. In: McCalpin, J.P. (Ed.), Paleoseismology. Elsevier, Amsterdam, p. 70.
Molinaro, M., Leturmy, P., Guezou, J.C., Frizon de Lamotte, D., Eshraghi, S.A., 2005. The structure and kinematics of the southeastern Zagros fold-thrust belt, Iran: from thin-skinned to thick-skinned tectonics. Tectonics 24, TC3007.
Motiei, H., 1993. Stratigraphy of Zagros. Geological Survey of Iran, Tehran.
Mouthereau, F., Tensi, J., Bellahsen, N., Lacombe, O., De Boisgrollier, T., Kargar, S., 2007. Tertiary sequence of deformation in a thin-skinned/thick-skinned collision belt: the Zagros Folded Belt (Fars, Iran). Tectonics 26, TC5006.
Mukherjee, S., Talbot, C.J., Koyi, H.A., 2010. Viscosity estimates of salt in the Hormuz and Namakdan salt diapirs, Persian Gulf. Geol. Mag. 147, 497–507.
Nissen, E., Tatar, M., Jackson, J.A., Allen, M.B., 2011. New views on earthquake faulting in the Zagros fold-and-thrust belt of Iran. Geophys. J. Int. 186, 928–944.
O'Brien, C.A.E., 1957. Salt diapirism in south Persia. Geol. Mijnbouw 19, 357–376.
Oberlander, T.M., 1985. Origin of drainage transverse to structures in orogens. In: Morisawa, M., Hack, J.T. (Eds.), Tectonic Geomorphology. Allen and Unwin, Boston, pp. 155–182.
Oveisi, B., Lavé, J., van der Beek, P., Carcaillet, J., Benedetti, L., Aubourg, C., 2009. Thick- and thin-skinned deformation rates in the central Zagros simple folded zone (Iran) indicated by displacement of geomorphic surfaces. Geophys. J. Int. 176, 627–654.
Perry, J.T.O.'.B., Setudehnia, A., Nars, M., 1965. South-East Fars Geological Compilation Map at 1:250,000. Iranian Oil Operating Companies, Geological and Exploration Division, Tehran.
Pizza, M., Ferrairo, M.F., Thomas, F., Tringali, G., Livio, F., 2023. Likelihood of primary surface faulting; updating of empirical relationships. Bull. Seismol. Soc. Am. 113, 2106–2118.
Player, R.A., 1969. Salt diapirs study. National Iranian Oil Company. Exploration Division, report 1146 (unpublished).
Ramsey, L.A., Walker, R.T., Jackson, J., 2008. Fold evolution and drainage development in the Zagros mountains of Fars province, SE Iran. Basin Res. 20, 23–48.
Richard, P., Naylor, M.A., Koopman, A., 1995. Experimental models of strike-slip tectonics. Petrol. Geosci. 1, 71–80.
Roberts, N.J., Evans, S.G., 2013. The gigantic seymareh (saidmarreh) rock avalanche, Zagros Fold-thrust belt, Iran. J. Geol. Soc. 170, 685–700.
Rodriguez, C.E., Bommer, J.J., Chandler, R.J., 1999. Earthquake-induced landslides: 1980–1997. Soil Dynam. Earthq. Eng. 18, 325–346.
Roustaei, M., Nissen, E., Abbassi, M., Gholamzadeh, A., Ghorashi, M., Tatar, M., Yamini-Fard, F., Bergman, E., Jackson, J., Parsons, B., 2010. The 2006 marc 25 fin earthquakes (Iran)-insights into the vertical extents of faulting in the Zagros simply folded belt. Geophys. J. Int. 181, 1275–1291.
Rowan, M.G., Lawton, T.F., Giles, K.A., Ratliff, R.A., 2003. Near-salt deformation in La Popa basin, Mexico, and the northern Gulf of Mexico: a general model for passive diapirism. AAPG (Am. Assoc. Pet. Geol.) Bull. 87, 733–756.
Ruh, J.B., Hirt, A.M., Burg, J.P., Mohammadi, A., 2014. Forward propagation of the Zagros Simply Folded Belt constrained from magnetostratigraphy of growth strata. Tectonics 33, 1534–1551.
Scheidegger, A.E., 1973. On the prediction of the reach and velocity of catastrophic landslides. Rock Mech. 5, 231–236.
Sepehr, M., Cosgrove, J.W., 2004. Structural framework of the Zagros fold–thrust belt, Iran. Mar. Petrol. Geol. 21, 829–843.
Sepehr, M., Cosgrove, J.W., 2005. Role of the Kazerun Fault zone in the formation and deformation of the Zagros Fold-thurst belt, Iran. Tectonics 24, TC5005.
Sherkati, S., Molinaro, M., de Lamotte, D.F., Letouzey, J., 2005. Detachment folding in the Central and Eastern Zagros fold-belt (Iran): salt mobility, multiple detachments and late basement control. J. Struct. Geol. 27, 1680–1696.
Sherkati, S., Letouzey, J., Frizon de Lamotte, D., 2006. Central Zagros fold-thrust belt (Iran): new insights from seismic data, field observation, and sandbox modeling. Tectonics 25, TC4007.
Sims, D., Ferrill, D.A., Stamatakos, J.A., 1999. Role of a ductile décollement in the development of pull-apart basins: experimental results and natural examples. J. Struct. Geol. 21, 533–554.
Smit, J., Brun, J.-P., Cloetingh, S., Ben-Avraham, Z., 2008a. Pull-apart basin formation and development in narrow transform zones with application to the Dead Sea Basin. Tectonics 27, TC6018.
Smit, J., Brun, J.-P., Fort, X., Cloetingh, S., Ben-Avraham, Z., 2008b. Salt tectonics in pull-apart basins with application to the Dead Sea Basin. Tectonophysics 449, 1–16.
Snidero, M., Muñoz, J.A., Carrera, N., Butillé, M., Mencos, J., Motamedi, H., Piryaei, A., Sàbat, F., 2019. Temporal evolution of the Darmadan salt diapir, eastern Fars region, Iran. Tectonophysics 766, 115–130.
Strom, A., 2015. Clustering of large bedrock landslides and recurrent slope failure: implications for land seismic hazard assessment of the Tien Shan-Djungaria region. International Journal of Geohazards and Environment 1, 110–121.
Talbot, C., Aftabi, P., 2004. Geology and models of salt extrusion at Qum Kuh, central Iran. J. Geol. Soc. 161, 321–334.
Talbot, C.J., Alavi, M., 1996. The Past of a Future Syntaxis across the Zagros, vol. 100. Geological Society, London, Special Publication, pp. 89–109.
Talbot, C.J., Jarvis, R.J., 1984. Age, budget and dynamics of an active salt extrusion in Iran. J. Struct. Geol. 6, 521–533.
Talbot, C.J., Pohjola, V., 2009. Subaerial salt extrusions in Iran as analogues of ice sheets, streams and glaciers. Earth Sci. Rev. 97, 155–183.
Talebian, M., Jackson, J., 2004. A reappraisal of earthquake focal mechanisms and active shortening in the Zagros mountains of Iran. Geophys. J. Int. 156, 506–526.
Tavakoli, F., Walpersdorf, A., Authemayou, C., Nankali, H.R., Hatzfeld, D., Tatar, M., Djamour, Y., Nilforoushan, F., Cotte, N., 2008. Distribution of the right-lateral

strike–slip motion from the main Recent Fault to the Kazerun Fault System (Zagros, Iran): evidence from present-day GPS velocities. Earth Planet Sci. Lett. 275, 342–347.
Thingbaijam, K.K.S., Mai, P.M., Goda, K., 2017. New empirical earthquake source-scaling laws. Bull. Seismol. Soc. Am. 107, 2225–2246.
Vergés, J., Emami, H., Garcés, M., Beamud, E., Homke, S., Skott, P., 2019. Zagros foreland fold belt timing across Lurestan to constrain Arabia-Iran collision. In: Saein, A.F. (Ed.), Developments in Structural Geology and Tectonics, vol. 3. Elsevier, Amsterdam, pp. 29–52.
Vernant, P., Nilforoushan, F., Hatzfeld, D., Abbassi, M.R., Vigny, C., Masson, F., Nankali, H., Martinod, J., Ashtiani, A., Bayer, R., Tavakoli, F., Chéry, J., 2004. Present-day crustal deformation and plate kinematics in the Middle East constrained by GPS measurements in Iran and northern Oman. Geophys. J. Int. 157, 381–398.
Walpersdorf, A., Hatzfeld, D., Nankali, H., Tavakoli, F., Nilforoushan, F., Tatar, M., Vernant, P., Chéry, J., Masson, F., 2006. Difference in the GPS deformation pattern of north and central Zagros (Iran). Geophys. J. Int. 167, 1077–1088.
Wells, D.L., Coppersmith, K.J., 1994. New empirical relationships among magnitude, rupture length, rupture width, rupture area, and surface displacement. Bull. Seismol. Soc. Am. 84, 974–1002.
Wesnousky, S.G., 1986. Earthquakes, Quaternary faults, and seismic hazard in California. J. Geophys. Res. Solid Earth 91 (B12), 12587–12631.
Wessel, B., 2016. TanDEM-X ground segment – DEM products specification document. EOC, DLR, Oberpfaffenhofen, Germany, Public Document TD-GS-PS-0021 46 pp. [Online]. Available:, Issue 3.2, 2016. https://tandemx-science.dlr.de/.
Wu, J., McClay, K., Whitehouse, P., Dooley, T., 2009. 4D analogue modelling of transtensional pull-apart basins. Mar. Petrol. Geol. 26, 1608–1623.
Youngs, R.R., Arabasz, W.J., Anderson, R.E., Ramelli, A.R., Ake, J.P., Slemmons, D.B., McCalpin, J.P., Doser, D.I., Fridich, C.J., Swan, F.H., Rogers, A.M., Yount, J.C., Anderson, L.W., Smith, K.D., Bruhn, R.L., Knuepfer, P.L.K., Smith, R.B., dePolo, C.G., O'Leary, D.W., Coppersmith, K.J., Pezzopane, S.K., Schwarts, D.P., Whitney, J.W., Olig, S.S., Toro, G.R., 2003. A methodology for probabilistic fault displacement hazard analysis (PFDHA). Earthq. Spectra 19, 191–219.
Zarei, M., Raeisi, E., Talbot, C., 2012. Karst development on a mobile substrate: Konarsiah salt extrusion, Iran. Geol. Mag. 149, 412–422.
Zarei, S., Faghih, A., Keshavarz, S., Zarei, E., 2023. Growth history and linkage pattern of fault-related folds deciphered from geomorphic analysis: a case study from the Dalan Anticline, Zagros Mountains, SW Iran. J. Afr. Earth Sci. 202, 104927.